
School of Engineering
Integrated Design Project 2018/19
Group: 33

COMMUTER LAMBDA AIR



Date: 10/02/19

Authors:

Vinush Vigneswaran (1390302)

Ho Yin Kwan (1806099)

Yuxiang Wan (1975429)

Tsz Wah Cheng (1700678)

Hanxuan Liu (-)

Tang Ji Hin (1864698)

Jiacheng Li (1727329)

CONTENTS

1. POWER DESIGN

- i. Qualitative Description
- ii. Quantitative Description: Specification Table
- iii. Model: The Simulation Model Diagrams
 - a. Overall Model
 - b. Power Generation
 - c. Power Conversion
 - d. Load
 - e. Control
- iv. Analysis
 - a. Inputs & Outputs
 - b. Energy Efficiency

2. LANDING GEAR DESIGN

- i. Qualitative Description
- ii. Quantitative Description
- iii. Model: The Landing Gear System
- iv. Analysis

3. STRUCTURAL DESIGN

- i. Qualitative Description
- ii. Quantitative Description
- iii. Model: Overall Structure and Load Conditions
- iv. Analysis: Design

4. APPENDIX

- i. Power Design
- ii. Landing Gear Design
- iii. Structural Design

5. REFERENCE

EXECUTIVE SUMMARY

The Commuter Lambda Air is a hybrid light aircraft, replacing conventional cars to travel. The aircraft allows three dimensional mobility to the general public, at a price tag similar to a luxury car. The Lambda Air is reliable, eco-friendly and sustainable. Lambda Air's business strategy consists of rolling out luxury, private aircraft, and evolving into a company which can produce affordable low-priced hybrid aircraft, to provide for humanitarian aid mission. . The design of the aircraft focused on modern and extremely energy efficient design, reducing mass, designing for minimal drag, highest safety rating and environmentally viable. The aircraft can hold up to 5 passengers and extra accessories. Lambda Air can be modified for load transport, such as food water and medical supply. The aircraft can cruise at low altitudes at around 200-250 mph, with a range of up to 1000 miles.

A hybrid power system is implemented in this design which contains hydrogen peroxide fuel cells, Li-battery and diesel fuel cells [1]. An alternator is used to charge the emergency battery. The design contains both AC and DC systems, power conversion methods are demonstrated in this design. Closed loop controlled methods are applied to stabilize the operations of the subsystems, and the behaviour of DC and AC loads is monitored [2]. Finally, the power efficiency will be calculated and discussed. Simscape mechanical and thermal domains are also used to simulate the actual behaviour of the landing gear system and the alternator system.

An extensive analysis of the landing gear has been conducted, as this essential for the safety during landing and take-off of the aircraft. The aircraft is able to conduct VTOL (vertical take-off and landing) using the 48 fans located on the wings, with 270° rotational capability. VTOL reduces the load on the landing gear, and significantly extends the life-cycle of the landing gear components. However, during emergency situations, such as failure in the fan or power, the aircraft will be able to use back-up power to autonomously land the aircraft using CTOL (conventional take-off and landing).

1. POWER DESIGN

(i) **QUALITATIVE DESCRIPTION** - This future aircraft design uses a hybrid power system which contains hydrogen peroxide fuel cells and an alternator circuit which contains diesel fuel cells and a starter battery [3]. The DC-AC inverter, DC-DC converter, AC-DC rectifier, and AC-AC step-down transformer are designed to satisfy the operational requirements of the loads [4]. The design of the avionics system and the selection of the DC motors have been carefully considered according to the sustainable and economic aspects. The engine inertia, engine friction, torque, rotational motor sensor, H-bridge, and thermal effects from Simscape physical domains are included to realistically simulate the actual behaviour of the landing gear subsystem [5]. The closed-loop control method, pulse width modulators are tested and verified by different loads and situations, which helps to minimize the safety issues of the power system. The emergency power is provided by both the extra battery and the alternator. The behaviour of avionics loads and DC motors, the actions of ignition and starter circuit, and the power efficiency of the system will all be monitored and analysed.

(ii) **QUANTITATIVE DESCRIPTION: SPECIFICATION TABLES**

Front/Back Wing DC Motor (30HP 240V 1750RPM Field:300V)	
Armature resistance and inductance [Ra (ohms) La (H)]	[0.2275, 0.002866]
Field resistance and inductance [Rf (ohms) Lf (H)]	[102.3, 20.82]
Field-armature mutual inductance Laf (H) :	0.401
Total inertia J (kg.m ²)	0.1239
Viscous friction coefficient Bm (N.m.s)	0.005219
Coulomb friction torque Tf (N.m)	3.164
Left/Right Flight Control DC Motor (20HP 240V 1750RPM Field:300V)	
Armature resistance and inductance [Ra (ohms) La (H)]	[0.4144,0.004895]
Field resistance and inductance [Rf (ohms) Lf (H)]	[105.9,27.65]
Field-armature mutual inductance Laf (H) :	0.4038
Total inertia J (kg.m ²)	0.08321
Viscous friction coefficient Bm (N.m.s)	0.004313
Coulomb friction torque Tf (N.m)	2.105
Alternator	
Back emf constant (V/rpm)	0.002
Rectifier diode total forward voltage drop (V)	1.2
Stator resistance represented on DC side (Ohm)	0.1
Thermal mass (J/K)	3*385
Initial temperature (deg C)	25
H-Bridge	
Enable threshold voltage (V)	2.5
PWM signal amplitude (V)	5
Reverse threshold voltage (V)	2.5
Braking threshold voltage (V)	2.5
Output voltage amplitude (V)	12
Total bridge on resistance (Ohm)	0.1
Freewheeling diode on resistance (Ohm)	0.1
Starter Motor	
Armature inductance (H)	1.00E-03
Stall torque (N*m)	10
No-load speed (rpm)	12000
Rated DC supply voltage (V)	12
Rotor inertia (kg*m ²)	0.001
Rotor damping (N*m/(rad/s))	0
Initial rotor speed (rpm)	0
Landing Gear Motor	
Armature inductance (H)	0.01
No-load speed (rpm)	4000
Rated speed (at rated load) (rpm)	2500
Rotor inertia (kg*m ²)	0.001
Rated load (mechanical power)	10W
Rated DC supply voltage (V)	12
Rotor inertia (kg*m ²)	0.0002
Rotor damping (N*m/(rad/s))	5.00E-06
Initial rotor speed (rpm)	0
Proton Exchange Membrane Fuel Cell	
Nominal operating point [Inom(A), Vnom(V)]:	[80,625]
Maximum operating point [Iend(A), Vend(V)]	[280,430]
Number of cells:	900
Nominal stack efficiency (%)	55%
Operating temperature (Celsius)	65
Nominal Air flow rate (lpm)	2100
DC-AC Inverter	
Device on-state resistance (Ohms)	1.00E-03
Snubber resistance (Ohms)	1.00E+06
Snubber capacitance (F)	inf

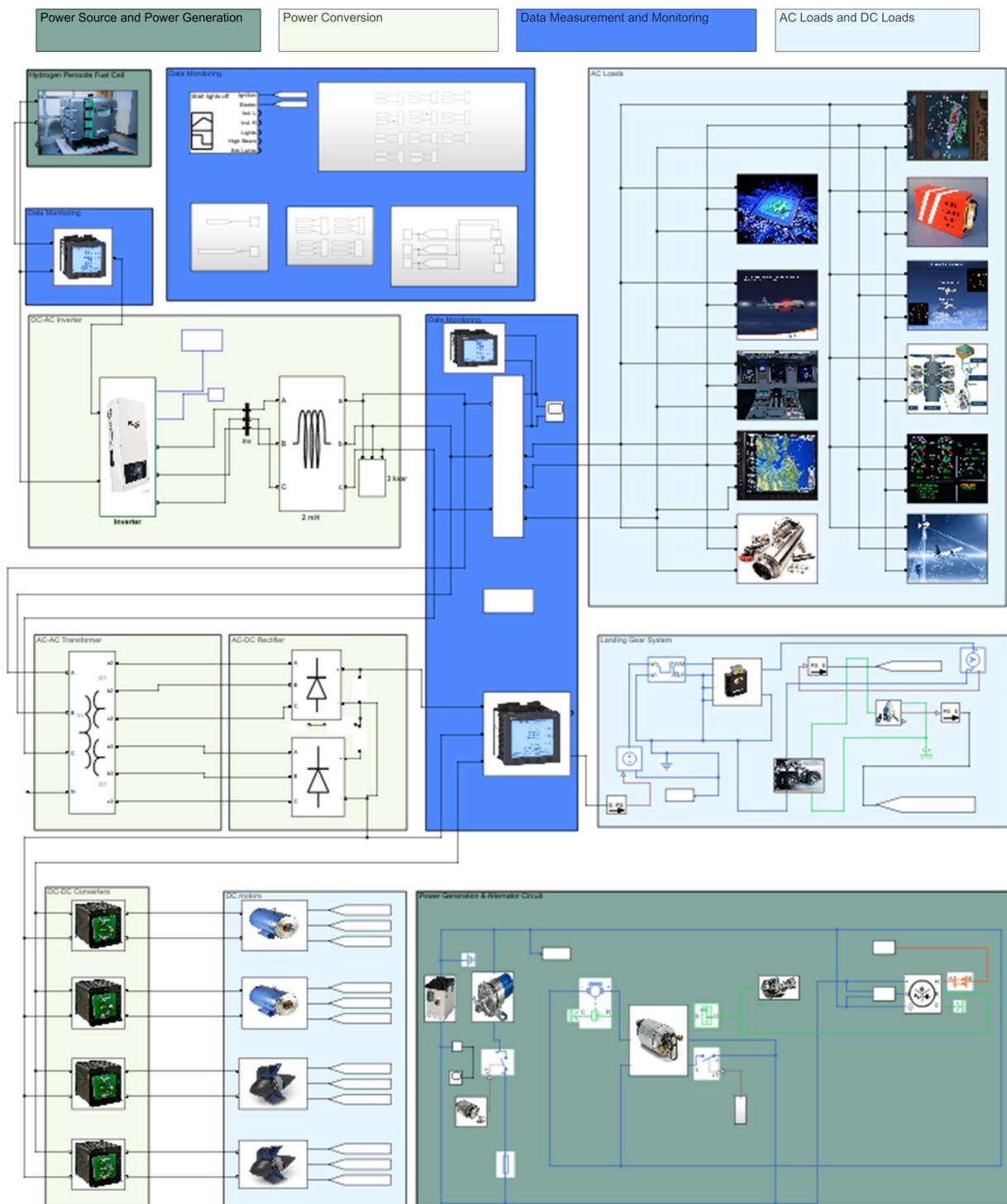
Three Phase Transformer	
Nominal power and frequency [Pn(VA) , fn(Hz)]	[4200, 600]
Winding 1 parameters [V1 Ph-Ph(Vrms) , R1(pu) , L1(pu)]	[200, 0.0002, 0]
Winding 2 parameters [V2 Ph-Ph(Vrms) , R2(pu) , L2(pu)]	[22, 0.0002, 0]
Winding 3 parameters [V3 Ph-Ph(Vrms) , R3(pu) , L3(pu)]	[22, 0.0002, 0]
Magnetization resistance Rm (pu)	500
Magnetization inductance Lm (pu)	5000

PWM Generator (Three-phase bridge (6 pulses))	
Mode of operation	Unsynchronized
Frequency (Hz)	2000
Initial phase (degrees):	90
Minimum and maximum values: [Min Max]	[-1,1]

Figure 1.1: Table showing datasheet for each power component.

(iii) MODEL: SIMULATION MODEL DIAGRAMS

Figure 1.2: Complete simulation model diagram



a. **POWER GENERATION** - Hydrogen peroxide fuel cell (**Figure 1.5**) is used for charging the majority of the components in the system due to its high efficiency, low operating noise, long operating time, simple maintenance and its ability to eliminate pollution [6][7]. A diesel engine is used during the lifting since it requires extra power. Then the engine will be turned off. A Li-battery is applied to the starter circuit, it will then be charged by the alternator whose rotor is rotated by the engine [8] as shown on Fig 1.3a and fig 1.3b.

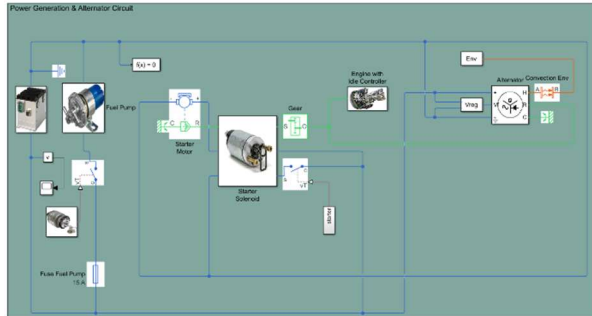


Figure 1.3a: Power Generation and Alternator Circuit

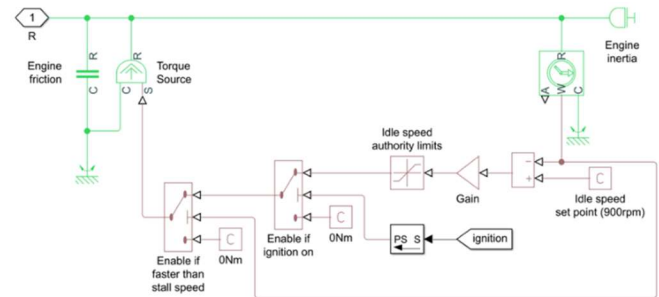


Figure 1.3b: Details of Engine Operation

The ignition system provides the spark to the fuel-air mixture since the spark is generated independently by magnetos from the electrical system, so even if the electrical system fails, the engine can still keep running [9]. In this simulation, the ignition signal is created in Simulink domain first then converted to Simscape physical domain. The engine inertia is assumed to be $0.05 \text{ kg} \cdot \text{m}^2$. The value from the Rotational Motion Sensor is controlled by the Idle speed authority limits, which is then used to generate the torque.

The starter is activated half a second after the ignition is triggered, which is shown in **Figure 1.4**.

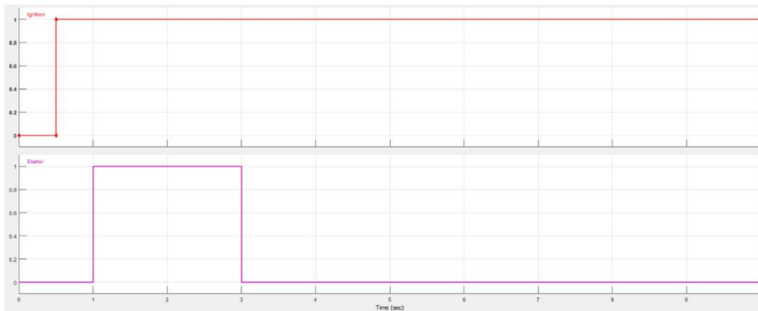


Figure 1.4: The ignition and starter relation

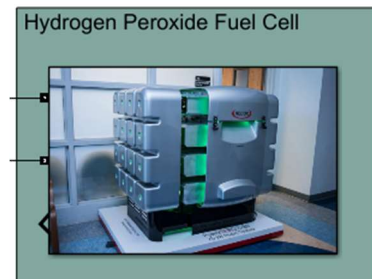


Figure 1.5: Hydrogen peroxide fuel cell

b. **POWER CONVERSION** - In this design, a DC/AC inverter (**Figure 1.6**), an AC/AC step down transformer (**Figure 1.7**), an AC/DC rectifier (**Figure 1.7**), and four DC/DC converters (**Figure 1.8**) are used to satisfy the power supply requirements of different loads. The functions of the 2-Level inverter are controlled by carrier-based Pulse Width Modulator, which in this design, the three-phase bridge is selected [10].

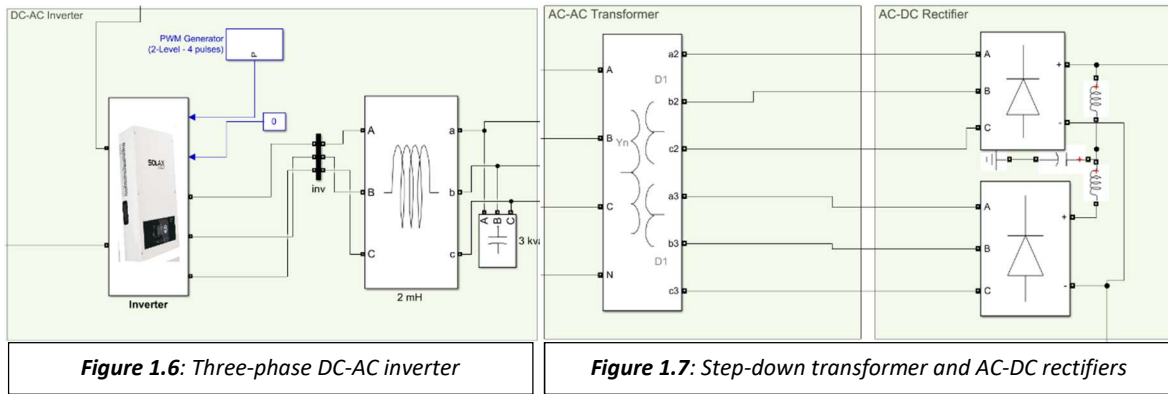


Figure 1.6: Three-phase DC-AC inverter

Figure 1.7: Step-down transformer and AC-DC rectifiers

A three-phase transformer is used to decrease the AC voltage, then the AC voltage is rectified to become DC voltage to supply the motor to control the landing gear [11]. Four DC/DC converters are used to supply the power to the electrical motors on the wings to supply kinetic energy as well as control the flying angle [12].

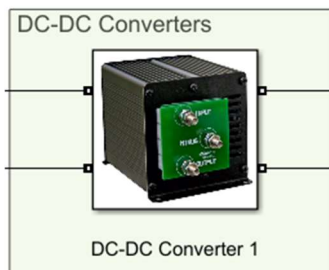


Figure 1.8 DC-DC converter

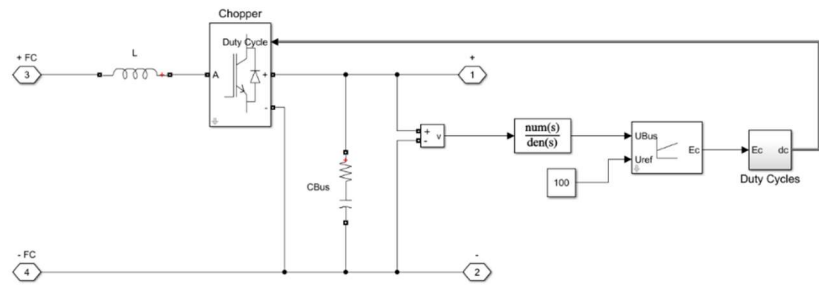


Figure 1.9: Details of DC-DC converter

c. LOAD -Both DC and AC loads are required in this design. DC loads include two flying control motors, 24 front wing motors, 24 back wing motors (**Figure 1.10**), and a landing gear motor (**Figure 1.12**). Simscape physical simulation is applied to the landing gear motor, which is controlled by s pulse width voltage signals and an H-bridge motor drive [13]. The current and rotational speed are measured by the current sensor and rotational motion sensor, which then can be converted to a Simulink signal and monitored from the scope. The 48 motors for providing thrust are simplified to 2 motor blocks which are front wing motor and back wing motor in order to increase the simulation speed. However, the power for these two motor blocks is the summation of the actual 48 motors. Two flying control motors are powered separately as shown in the diagram. The behaviour of rotational speed, armature current and electrical torque of the motors can be monitored from the scopes (**Figure 1.11**).

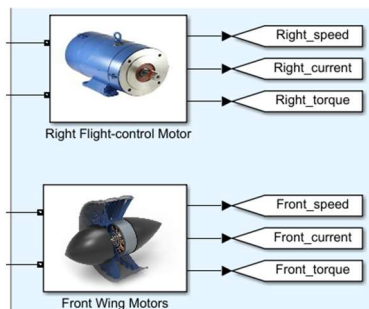


Figure 1.10: Flight-control motors and Front/Back Wing motors.

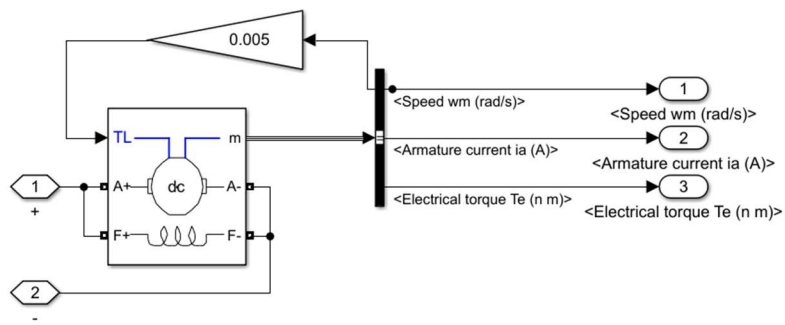


Figure 1.11: Details of a DC motor with closed-loop control.

AC loads (**Figure 1.13**) include communication system, navigation system, lighting system, flight-control system, monitoring and warning system, fuel system, collision-avoidance system, flight recorders, weather system, heating system, and aircraft management system [14] [15]. All the AC loads can be monitored.

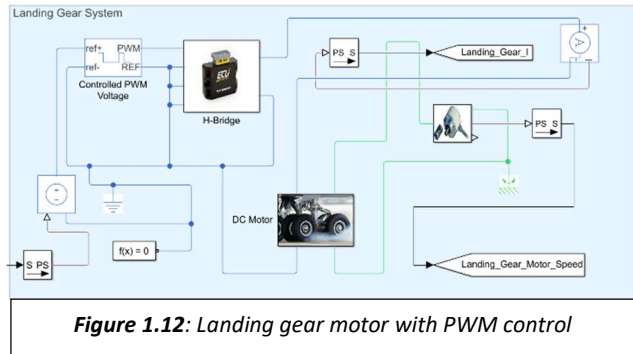


Figure 1.12: Landing gear motor with PWM control

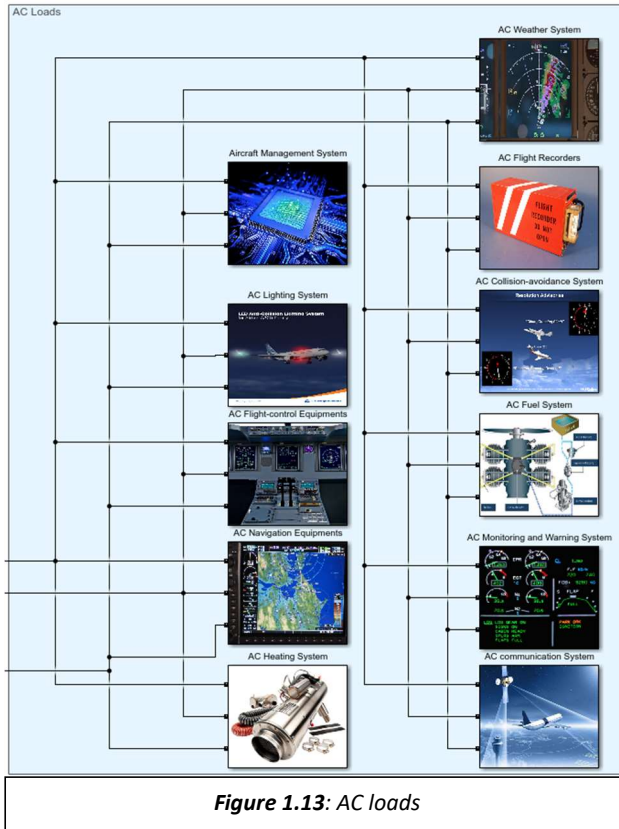


Figure 1.13: AC loads

d. CONTROL - Pulse Width Modulators are used to control the inverter and the landing gear H-bridge (**Figure 1.14 & Figure 1.15**). The closed-loop control method is applied to other motors (**Figure 1.11**). The ignition system is implemented in the alternator circuit. For the inverter, the pulse width generator produces firing pulses to control the diode pairs inside the inverter, the carrier-based two-level PWM method is implemented. In this design, the three-phase bridge is selected to meet the requirements for powering the AC loads. [16] The frequency is set to 2000 Kz, and the initial phase degree is 90 [17].

For the controlled PWM voltage of the landing gear H-bridge, the output will be 0 if the pulse is low. If the pulse is high, the output will be 5V. The pulse width frequency is set to be 4000 H Hz. The closed-loop control method is implemented to all the DC motors to stabilize the operations thus improve the

accuracy of the speed and flying-angle control. The closed-loop system compares the feedback value with the desired value, once the error is detected, corrections will be applied [18] [19].

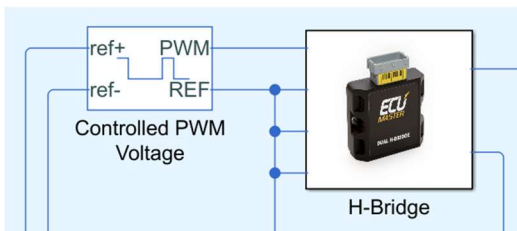


Figure 1.14: H-bridge controlled by PWM

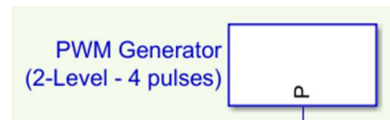


Figure 1.15: PWM Generator for controlling the inverter

(iv) ANALYSIS: SIMULATION RESULT



Figure 1.16: Total power input



Figure 1.17: Total power of DC loads



Figure 1.18: Total power of AC loads

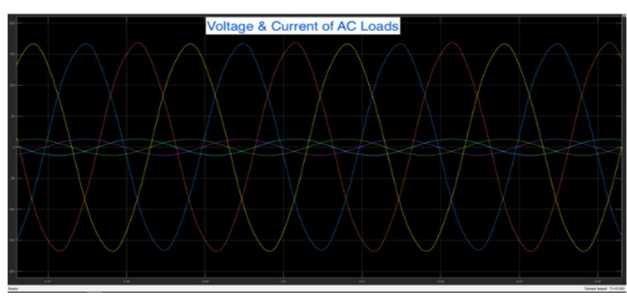


Figure 1.19: Voltage & Current of AC loads

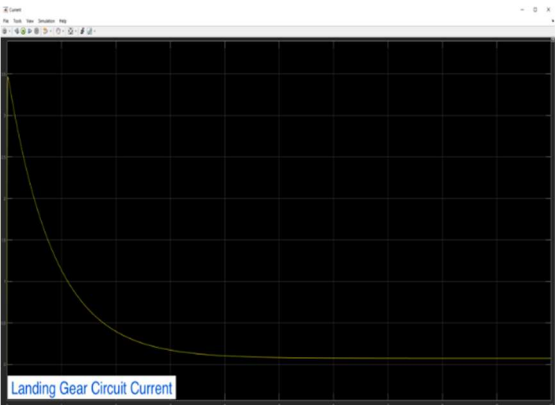


Figure 1.20: Landing gear circuit current

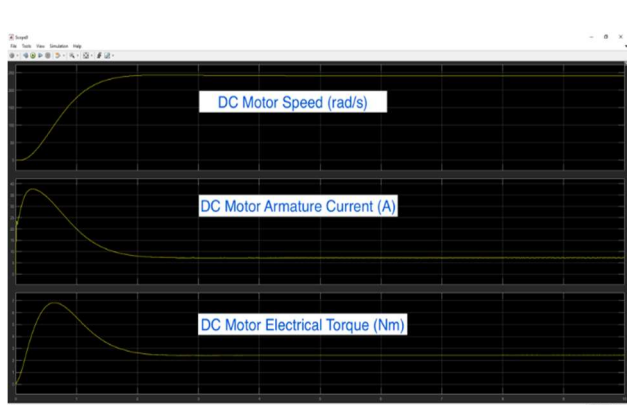


Figure 1.21: DC motor monitoring (Rotational Speed, Armature current, Electrical torque)

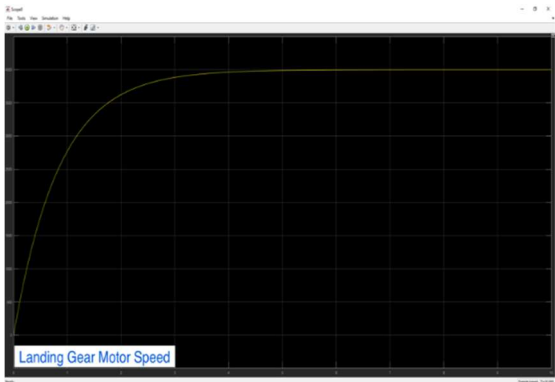


Figure 1.22: Landing gear motor speed



Figure 1.23: Power efficiency

a. INPUTS AND OUTPUTS - Total power input is measured using a voltage measurement, a current measurement, and a power measurement. As shown in the graph below, the total power input from the fuel cells is approximately 820kW (**Figure 1.16**). The total power consumed by the AC and DC loads varies against time. More power is consumed to start the DC motors, then their power requirement decreases dramatically (**Figure 1.17**) [20]. On the other hand, for AC loads, the sum of their power output increases against time (**Figure 1.18**).

b. AC LOADS MONITORING – **Figure 1.19** shows that the power generated by the hydrogen peroxide fuel cell is converted to a three-phase AC source.

c. DC LOADS MONITORING - The behaviour of the DC motor is shown in **Figure 1.20**, **Figure 1.21**, and **Figure 1.22**. Initially, the motor was not activated, therefore at the beginning the electrical torque is higher. Then the motor starts accelerating until its limit. The armature current decreases as the speed increases [21].

d. ENERGY EFFICIENCY - As shown in **Figure 1.23**, the power efficiency remains approx. 60% which can be concluded as follows:

- During the power conversion process, the waveform is filtered by capacitors, resistors and a transformer. In order to allow the basic parts of the waveform to successfully reach the output, normally a low pass filter is applied. These electronics might consume a considerable amount of power during the conversion. In this design, the three-phase inverters are implemented thus the losses are even higher [22].
- For DC motors, the non-ideal features include field, viscous friction and Coulomb friction torque [23].
- For AC loads, extra resistors and inductors are used to simulate the losses caused by active and reactive power in the protection devices, cables, and wires.
- The losses in the alternator include:
 - a) Friction losses: due to the rotor or the blowers.
 - b) Core losses: hysteresis and eddy currents
 - c) Stray load losses: due to magnetic flux distribution, harmonic and eddy currents [24] [25].

2. LANDING GEAR DESIGN

(i) QUALITATIVE DESCRIPTION

a. LANDING GEAR SYSTEM - The main objective of this design of the landing, is to utilise light materials in order to achieve efficient flight, whilst reducing cost of manufacturing. As this is a small aircraft, a retractable landing gear would decrease the drag significantly during flight, as the landing gear accounts for approximately 18% [refer to Appendix calculation] of the frontal area. The aircraft is able to conduct VTOL (vertical take-off and landing), which reduces the load on the landing gear, and significantly extends the life-cycle of the landing gear components. However, during emergency situations, such as failure in the fan or power, the aircraft will be able to use back-up power to autonomously land the aircraft using CTOL (conventional take-off and landing). The following report assumes conditions of the landing gear during CTOL.

b. SUB-COMPONENTS OF LANDING GEAR

Sub-components	Description & Selection Criteria
ELECTRO-MECHANICAL LINEAR ACTUATORS (EMA)	Essential for retractable landing gear function (release, locking & retracting). EMA has a relatively low mass compared to conventional hydraulic actuators, as it does not consist of any fluid and allows the elimination of local hydraulic circuits, therefore significantly reduces wear of the materials. Trade-off for EMA was the jam susceptibility, due to drive and roller screw becomes stacked.
HYDRAULIC BRAKING DEVICE	Reliable and efficient, as it is able to absorb a high magnitude of force. Compared to mechanical braking system, hydraulic systems, have lower maintenance requirements, due to reduced wear from mechanical parts. The aircraft's hybrid power system, allows for the efficient use of regenerative braking to recharge the battery from kinetic energy during conventional take-off and landing. As it is a sealed system, less energy is lost to gear systems, allowing the force to be directly applied to the breaking calliper.
OLEO-PNEUMATIC SHOCK ABSORBER	Absorbs and dissipates the landing impact energy to avoid transferring them to the aircraft structure, therefore causing damage. Oleo-pneumatic shock strut have minimal weight and is capable of efficiently damping heavy impact loading conditions. As the aircraft lands, the impact pressure generated by the wheels and ground will forces the hydraulic fluid, up through the orifice hole to the top cylinder (attached on the aircraft) and mix with nitrogen, which dissipates the energy as heat.
POWER STEERING	Power steering is integrated into landing gear, in order to facilitate taxiing and manoeuvrability during ground operations. Electric power steering systems are very reliable due to the absence of fluids (hydraulic), therefore minimal maintenance is required. Thus provides highly accurate controllability and response rate. The system consists of two antagonistic actuators pushing and pulling the steering spindle to rotate the wheel.
WHEEL & TYRE	The aircraft wheel and tyre are crucial component of the landing gear system, as they support the weight of the aircraft during taxi and ground operations, as well as acting as dampers during take-off and landing. The design parameters for the wheel material includes, lightweight and high tensile strength, which is satisfied by specific Aluminium alloys. The wheel consists of bearing rollers and grease retainer in the central axle, to minimise friction. The tyre must be large enough to include the braking assembly.

Figure 2.1.1: Table shows description and required criteria of main sub-components of the landing gear

c. METHODS OF INTERFACING & MATERIAL COMPOSITION

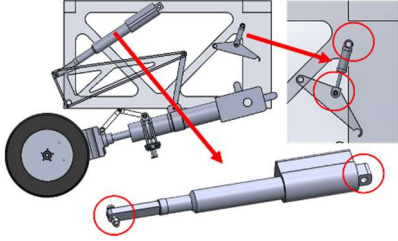
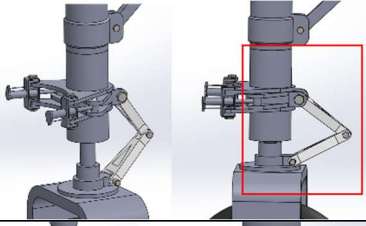
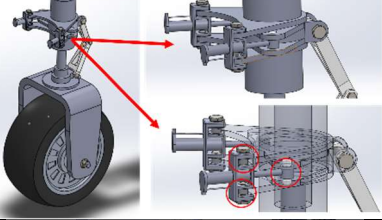
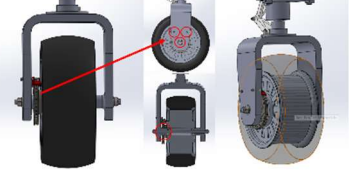
Sub-components	Method of Interfacing	Illustration
Electromechanical linear actuators	The actuators require movement around an axis in order to facilitate frictionless landing gear retraction, extension, up and down lock. Therefore there is a pivotal connection with the landing gear chassis, with bearing attachment. The dynamic end of the actuator is connected via screws, bearing fasteners and lubrication.	
Oleo-pneumatic shock absorber	The main shock absorber from the supplier requires an additional casing to interface with the strut. There is an internal press fit, and 4 screw fits. The brace is attached as shown, with screws.	
Power steering	The steering is controlled by actuators, connected to a steering spindle. The static part is connected to the uppermost and lowermost spindle with screw, washer and bolt. The dynamic part is connected to inner spindles.	
Hydraulic braking device & Wheel and tyre	The brake calliper is connected to the fork via two screws (position) and one screw (axle). The tyre is fitted into grooves on axle casing.	

Figure 2.1.2: Table shows methods of interfacing and the main material composition

d. COMERCIAL SUPPLIERS INFORMATION

Supplier (Product Code)	Design Parameters	Selected Product Suitability Analysis	Industrial Production & Maintenance
Electro-mechanical linear actuators (incl. power steering) Thomson Linear Motion [28] (HD12B017-0100CNO1EES)	Low mass, accurate control, high dynamic load, internal brake system, fast travel rate, function at varying environmental temperature, environmental protection.	Suitable: Relatively low mass, high precision. Consists of temperature monitoring and reasonable voltage tolerance. Trade-off: Physical model casing must be slightly altered. Modification to wire and front connector required.	EU Certified and CE compliant. Batch production available, however transported from US. Composite Material: Copper, Steel, Zinc, Plastic
Hydraulic braking device Tolomatic [32] (H220I Series)	Calliper disk brakes, low mass, withstand high pressure, and provide high torque, cheap, high-grade friction material, suitable material for disk, high efficiency.	Suitable: Low mass and low cost – cast iron. Parameters accommodates tyre and disk. Single acting with floating bracket (can be mounted to the nose shaft). Trade-off: Low lifespan and routine maintenance required.	High production available. Suitable for front landing gear and back braking system – bulk purchase can reduce costs. Manufactured and distributed in the UK. Maintenance system must be integrated within aircraft. Yearly brake check required – cheap to exchange parts. Material: Nodular Cast Iron
Oleo-pneumatic shock absorber	High energy capacity, withstand high reacting force,	Suitable: High operating temperature range, and very	Manufactured in the US, therefore transportation costs must be

Ace Controls Inc. [29] (SCS38-150)	minimal extension (reduce landing gear height), withstand impact velocity, low mass and loss cost, high operating temperature. Creep speed conditions for quality testing.	compact design, material composition optimised for corrosion and thermal resistance. Excellent damping medium and results. Adheres to quality testing conditions. Trade-off: High cost and maintenance required.	considered. Can only be purchased in small batches, however the company is undergoing an enlargement scale-up process, and will be able to supply required quantity. Composite Material: Steel coating & hard chrome plated steel
Brake Disc Comline Auto Parts [30] (ADC1215V)	High grade friction material, low density material, low mass, low cost, perform under severe conditions, high performance under varying load, high temperature range.	Suitable: Low cost, low mass, easy to manufacture, simple design. Trade-off: Surface finish altered for safer braking due to mass of this landing gear.	Easy to manufacture, and large production available. Material: Cast Iron

Figure 2.1.3: Table shows the suppliers, product code, design parameters for selection process and material composition for each out-sourced part.

(ii) QUANTITATIVE DESCRIPTION

a. DESIGN PARAMETERS: SUB-COMPONENTS AND SUB-SYSTEMS OF LANDING GEAR

Sub-system 1: Landing Gear Dynamics

Electromechanical Actuators: Landing Gear Retraction and Deployment [28]		Electromechanical Actuators: Up & Down Lock [28]	
Type:	Electromechanical	Type:	Clutch Electromechanical
Supplier (Product Code):	Thomson (HD12B160-0400CNO1EEM)	Supplier (Product Code):	Thomson (AA22-05A65M0M0N)
Dimensions (Retracted): L x W x H	627.6 x 77 x 148 mm	Dimensions (Retracted): L x W x H	216.7 x 76.2 x 148 mm
Mass:	8.5 kg	Mass:	6 kg
Nominal Stroke:	400 mm	Nominal Stroke:	50 mm
Voltage Tolerance:	9 – 16 VDC	Voltage:	230 VAC
Current Draw:	3 – 20 A	Current Draw:	-
Max Dynamic Load:	16000 N	Max Dynamic Load:	1100 N
Max Static Load:	18000 N	Max Static Load:	11350 N
Interfacing Components:	15 mm diameter hole on actuator connected via bearing (fig 2.10) to drawbar. Connected by M15 screw.	Interfacing Components:	12 mm diameter hole on actuator connected via bearing (fig 2.10) to drawbar. Connected by M12 screw.

Figure 2.1.4: Table shows quantitative description of actuators

Sub-system 2: Braking System

Braking System Hub & Disc		Calliper Bracket	
Type:	Ventilated Disc	Type:	Single Acting Bracket
Supplier (Product Code):	Tolomatic (0803-1214)	Supplier (Product Code):	Tolomatic (H220SAFCIG)
Dimension of disc (Radius, Thickness):	140 mm, 30 mm	Dimensions of Calliper Bracket (L x W x H)	177.8 x 880 x 55.0 mm
Mass:	6.99 kg	Dimensions of Disc Insert (Radius, Max Thickness)	152, 60 mm
Thermal Dissipative Capacity:	25.2 MJ at a speed of 1800 RPM (Linear Relationship)	Mass:	4.76 kg
Interfacing Components:	The disk will be inserted into calliper bracket. The 5 holes will be connected to a washer, and then fastened on to axle (Screws M10 x 10 mm). The disk	Dynamic Brake Torque:	3955 N.m at a max pressure of 1000 PSI
		Static Dynamic Brake Torque:	2485 N.m at a max pressure of 1000 PSI
		Interfacing Components:	M8 x 30mm bolts use to fasten onto fixed member (landing gear strut). Parallel

	must be aligned parallel the wheel and the bracket to reduce friction.		alignment, and fixed when brake is released. Bleed pressure before use. Insert the disk into calliper gap.
--	--	--	--

Figure 2.1.5: Table shows quantitative description of braking system

Sub-system 3: Oleo- Pneumatic Shock Absorber

Shock Absorber		Strut Structural Parameter	
Type:	High Rack Damper	Type:	Cylinder Strut
Supplier (Product Code):	Ace Controls (SCS38-150)	Manufacture Code	UOB-CC259
Dimensions (Retracted): L x W x H	320 x 160 x 160 mm	Dimensions: Radius, Height	55 mm, 545 mm
Mass:	16.0 kg	Material:	Aluminium, 7049, T73
Nominal Stroke:	150 mm	Compressive Yield Strength:	352 -455 MPa
Max Reaction Force	80000 – 191400 N	Mass:	3.7 kg
Filling Pressure	2 MPa	Interfacing Components:	The cylinder strut is connected to the shock absorber on one end, and the other end is connected landing gear chassis pivot system. The strut holder and the strut is interfaced with 6 screws (M15 x 20) on the disc face of the strut.
Interfacing Components:	The shock absorber must be loaded symmetrically (centrally). The piston must be fitted into the landing gear main strut. Either end of the piston must be connected onto the interface on the strut, with the holes aligned. The M18 x 25 screw must be tightened with a bolt & washer.		

Figure 2.1.6: Table shows quantitative description of shock absorber.

Sub-system 4: Power Steering

Steering Actuators		Main shaft connectors (steering)	
Type:	Clutch Electromechanical	Type:	Steering Spindle
Supplier (Product Code):	Thomson (AA42-21B65M0M0B)	Manufacture Code:	UOB-CC260
Dimensions (Retracted): L x W x H	216.7 x 76.2 x 148 mm	Dimensions: L x W x H	205 x 205 x 10 mm
Mass:	6.8 kg	Material:	Cast Iron, gray, flake graphite, EN GJL 250
Nominal Stroke:	50 mm	Tensile Strength:	250 – 350 MPa
Voltage:	400 VAC	Mass:	0.97 kg
Dynamic Load:	6800 N	Interfacing Components:	The main hole on the spindle is for the insertion of the landing gear strut. The two side holes, requires M16 screws to be inserted and fastened to the steering actuators. The same spindle is also attached below the two steering actuators.
Static Load:	18000 N		
Interfacing Components:	10 mm diameter hole on actuator connected via bearing (fig 2.10) to the steering spindle. This part needs an additional casing to fit the strut criteria, the casing will consist of back holes, which will connect M10 screw to the spindle.		

Figure 2.1.7: Table shows quantitative description of actuators

Sub-system: Wheel and Tyre

Wheel		Tyre	
Type:	Bias Tire	Type:	Bias Tire
Manufacture Code:	UOB-CC261	Supplier:	Aero trainer (AD4D4)
Material:	Aluminium 7050 T7451	Material:	Polyurethane rubber
Dimensions: (Radius, Width)	175, 200 mm	Dimensions: (Radius, Width)	175, 127 mm
Weight:	10 kg	Weight:	2 kg
Dynamic Load:	34 kN	Interfacing Components:	Insert the tyre on top of the wheel. Ensure tyre edge falls into groove. Attach removable flange and fasten using 4 screws and bolts.
Static Load:	37 kN		
Interfacing Components:	Remove the removable flange and the lock ring. Insert the rim of the wheel into the axle (on top of the bearing). Ensure full alignment for tyre insertion.		

Figure 2.1.9: Table shows quantitative description of wheel and tyre

Structural Assembly Connectors

Bearings		Shaft Couplings	
Supplier:	RS Components	Supplier:	RS Components
Bearings required:	<p>LINEAR BEARING (R065822540) Outer Radius: 35 mm Inner Radius: 25 mm Thickness: 40 mm</p> <p>BALL BEARING (505-647) Outer Radius: 200 mm Inner Radius: 95 mm Thickness: 45 mm</p> <p>FLANGED Bearing (750-8924) Inner Radius: 60 mm Length x Width: 187 x 187 mm Depth: 73.7 mm</p>	Shaft Coupling:	<p>UNIVERSAL JOINT (RS 790-6693) Joint: Single Outer Diameter: 16 mm Bore: 8 mm Overall Length 40 mm Peak Torque: 600 N.m</p> <p>NEEDLE ROLLER JOINT (RS 790-6823) Joint: Double Outer Diameter: 50 mm Bore: 25 mm Overall Length 163 mm Peak Torque: 200 N.m</p>

Figure 2.1.10: Table shows quantitative description of bearings and shaft coupling

(iii) MODEL

a. Integrated Landing Gear

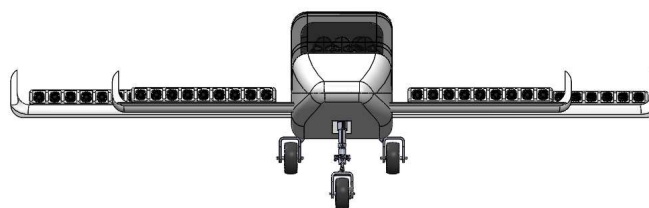


Figure 2.1.11 – Front view of the integrated landing gear

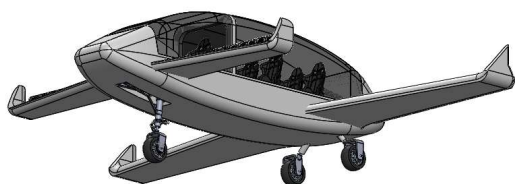


Figure 2.1.12 – Bottom view of the integrated landing gear

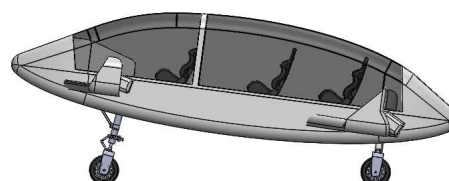


Figure 2.1.13 – Side view of the integrated landing gear

b. Landing Gear Retraction Dynamics

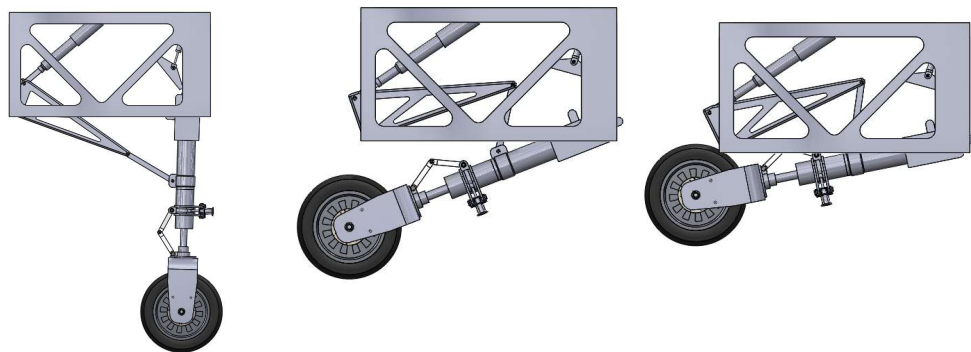


Figure 2.1.14 – Three stages of retraction of the landing gear (fully extended and fully retracted)

c. Landing Gear Overall Dimensions

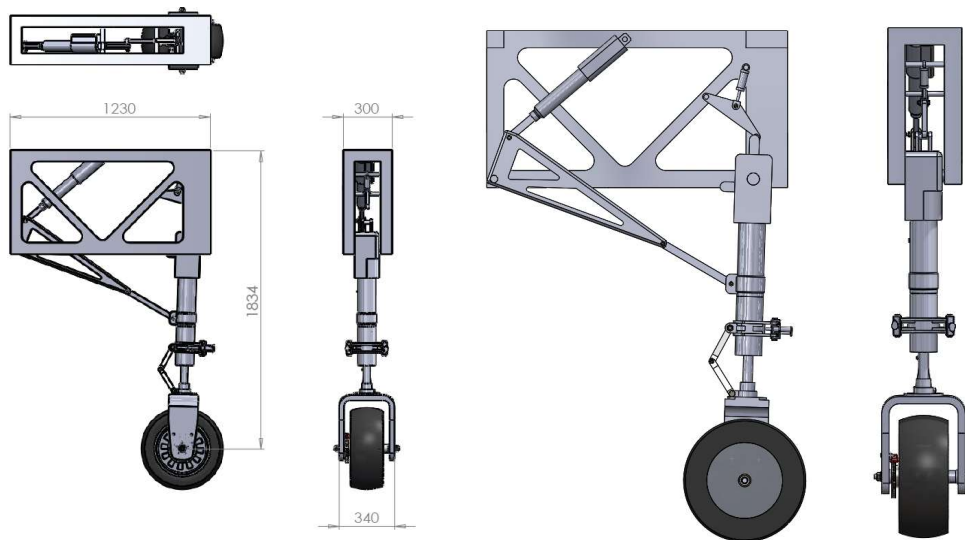


Figure 2.1.15 – Dimensions of the landing gear

Figure 2.1.16 – Cross-sectional view of landing gear

d. Exploded view of landing gear and tyre & wheel sub- system

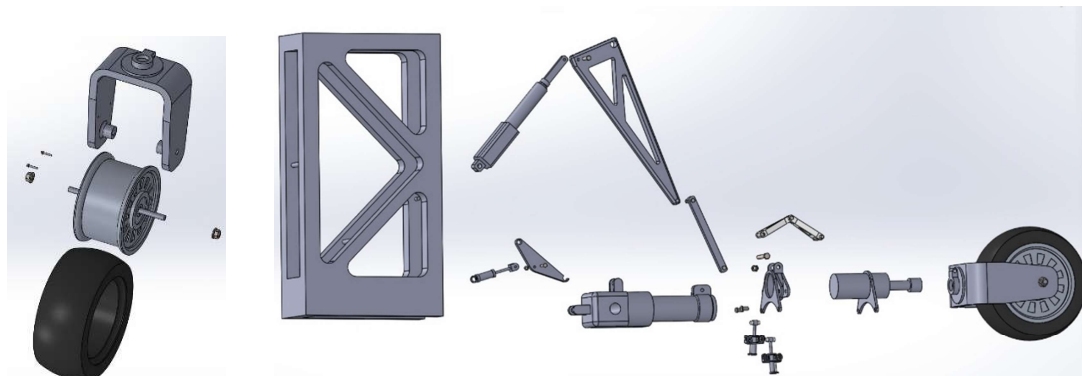


Figure 2.1.17 – Exploded view of tyre and wheel.

Figure 2.1.18 – Exploded view of landing gear chassis and sub-components.

SUB-COMPONENTS AND INTERFACING HAVE BEEN SHOWN IN FIGURE 2.1.2/

(iv) ANALYSIS

a. LANDING CONFIGURATIONS – The land gear configuration is essential for calculating many other design parameters such as static and dynamic load for the steering and shock absorber. The landing gear has been positioned to minimise load, whilst distributing the internal, external and structural components of the aircraft. The centre of gravity and moment calculations were conducted using the following equation:

$$(Eqn 1.1) \sum M = F_1x_1 + F_2x_2 \dots = 0$$

Where M = moment (N.m), F = force (N) and x = distance from pivot point.

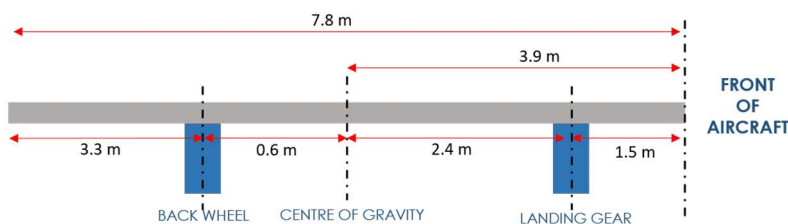


Figure 2.2.1 – The diagram shows the arrangement of the landing gear

Part	Mass (kg)	Distance from front (m)
Fuselage	1050	3.9
Passenger	400	4.3
Battery	540	3.9
Front Wing	610	1.5
Back Wing	940	6
Fuel	50	6
Engine	280	1.3
Landing Gear Front	200	1.5
Landing Gear Back	200	4.5
Total	4270	7.8

Figure 2.2.2 – The table shows the distance of the main components with relatively significant mass.

b. STATIC LANDING GEAR LOAD CALCULATIONS - When the aircraft is static on the ground, the sum of moment acting on the aircraft is 0; therefore using equation 1.1 and 1.2, the following can be obtained:

$$(Eqn 1.2) \sum F_x = 0, \quad \therefore R_{FRONT} + (2 \cdot R_{BACK}) = W_{AIRCRAFT}$$

Where R_{FRONT} = Reaction force at the front landing gear, R_{BACK} = Reaction force at the back wheels and $W_{AIRCRAFT}$ = Weight of aircraft.

$$(Using Eqn 1.1) (F_{FRONT} * 2.4) = (2 * F_{BACK} * 0.6)$$

Where F_{FRONT} and F_{BACK} are the forces acting on the front landing gear and landing gear, due to the position of the weight of the aircraft.

According to equation 1.2, the sum of the reaction forces equals the weight of the aircraft (Max mass = 4500 kg). Therefore, the following parameters are shown/calculated:

Maximum Weight of Aircraft: **44131N**, Force acting on **Landing gear: 14,715 N**, Force acting on back strut and wheel: **14,715 N** at each strut.

c. DYNAMIC LANDING GEAR CALCULATIONS – The dynamic landing gear calculations are essential to calculate maximum force require by the shock absorbers and tyre. If the thruster were directed perpendicular to the aircraft’s motion, minimum speed required to maintain the flying height can be calculated using the following two equations.

$$(Eqn 2.1) \text{Lift force, } F_L = \frac{1}{2} \rho C_L A V^2 \quad (Eqn 2.2) \text{Drag Force, } F_d = \frac{1}{2} \rho C_D A V^2$$

Where $p = \text{Density of air } (1.225 \text{ kg/m}^3)$, $C_L = \text{Lift coefficient}$, $A = \text{Area of total wing span } (m^2)$, $V = \text{Speed of the aircraft relative to the flow } (m/s)$.

For the aircraft to maintain a constant height, the Lift force must be equal to the weight of the aircraft. Drag force acting on the main body can be estimated by first estimating the wing speed using equation 2.3.

(Eqn 2.3) $U_{average} = U_{10} \left(\frac{z}{10}\right)^\alpha$ (Using Eqn 2.2) $F_d = 10620N$

Where, U_{ave} is the average wing speed at target height, U_{10} , wind speed at 10 m height is 30 km/h, Z is the height of the aircraft = 310 m and terrain index $\alpha = 0.3$. The average wind speed at 310 m height will be 23.3 m/s. Maximum flight speed is 250km/h, and our aircraft had a drag coefficient of 0.7.

Flight speed (km/h)	Flight Speed (m/s)	Lift Coefficient	Drag Coefficient	Drag force on wings (N)	Angle of attack ($^\circ$)	Drag Force on body	Total Drag Force (N)
180	50.55	1.45	0.15	4566.7	15.6	6734.4	11301.1
200	55.55	1.2	0.095	3495	10.8	7679.1	11174.1
250	69.44	0.77	0.04	2303.96	1.4	10620	12924.0

Figure 2.2.3 – Table showing total drag force acting on the wings, body and aircraft.

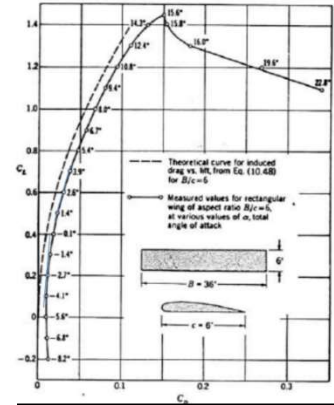


Figure 2.2.4 – Lift coeff against Drag coeff corresponding to an aspect ratio of 6

(Eqn 2.4) $\alpha = \theta + \varphi$, $\alpha = 15.71^\circ$

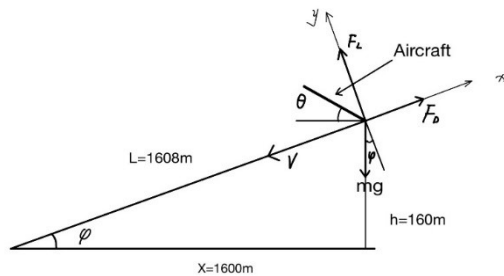


Figure 2.2.3 – The diagram shows the free body diagram of the trajectory of the aircraft, as well as the gliding ratio.

Where $\alpha = \text{angle of attack}$, $\theta = 10^\circ$ (angle of the aircraft to the ground), $\varphi = 5.71^\circ$ (angle of glide ratio 1:10).

The aircraft is assumed to land from lowest altitude in the UK [31], which is 160 m above ground. Therefore using the 1:10 gliding ratio, the horizontal distance covered from landing preparation would be 1600 m. Therefore, the glide distance of the aircraft, L , is 1608m

(Using Eqn 2.1) $F_L = 44166$ (Using Eqn 2.2) $F_D = 4569N$

Whereby the following variables were used in Eqn 2.1 and 2.2: $V = 50.5m/s$ represents the speed that aircraft starting gliding and $A = 19.5m^2$ is the area of all the wings, and from Fig 2.2.4, $C_D = 0.15$ and $C_L = 1.45$. The acceleration of the aircraft in the direction of motion is:

(Eqn 2.5) $F_L = W \cdot \cos(\varphi)$ (Eqn 2.6) $a_x = \frac{mg \cdot \sin(\varphi) - F_D}{m}$, $a_x = -0.04m/s^2$

Where a_x represents the acceleration in x-axis, and F_L is equal to the mass perpendicular to the line of motion (refer to Fig 2.2.3).

The velocity close to ground reduces to:

$$(Eqn 2.7) V_{landing}^2 - V^2 = 2a_1L, \quad V_{landing} = 49.2m/s$$

$$V_x = V_{landing} \cdot \cos(\varphi) = 49m/s, V_y = V_{landing} \cdot \sin(5.71) = 4.9m/s$$

Where V_x represents the speed of sliding on the ground and V_y is the vertical speed of landing.

The acceleration of the front gear when landing can be calculated as follows:

$$(Using Eqn 2.1) F_{L2} = 34412N, F_{D2} = 2724N$$

$$(Using Eqn 2.6) a_2 = 2.163m/s^2$$

Where F_{L2}, F_{D2}, a_2 represents lift force, drag force and the acceleration of central gravity when aircraft is sliding on the ground. $C_{L2} = 1.2$ and $C_{D2} = 0.095$ when the angle of attack is 10° , So when the aircraft is sliding on the ground.

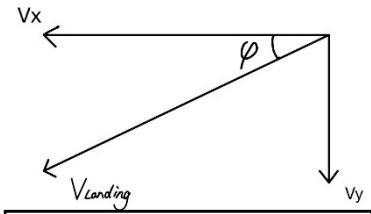


Figure 2.2.4 – The components of the landing velocity

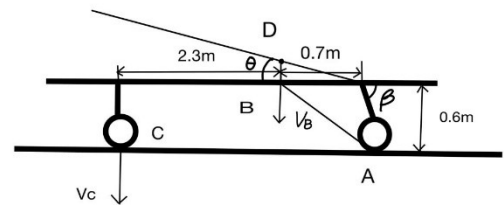


Figure 2.2.5 – The components of the landing velocity

$$V_B^2 = 2a_2L_{BD} \quad V_B = \sqrt{2 \times 2.163 \times 0.1215} = 0.725m/s$$

Where, $L_{BD} = 0.7m \times \sin(10^\circ) = 0.1215m$, the distance is that central gravity moves before front wheel touches the ground, V_B is the velocity of centre of gravity when front wheel get touch with ground. Thus, $\beta = 84^\circ$ which is the angle between chassis and back wheel, $L_{AB} = 0.97m$ and $L_{AC} = 3m$, V_C is the vertical speed of front wheel when it touch with ground, therefore:

$$V_C = \frac{L_{AC}}{L_{AB}} \cdot V_B = \frac{3}{0.97} \times 0.725 = 2.24m/s$$

d. SHOCK ABSORBER – The dynamic landing gear calculations conducted provides the main parameters for the shock absorber. The design of shock absorber stroke can be derived from the kinetic energy equation, and the maximum velocity can be calculated by the following equation:

$$(Eqn 3.1) \text{ Stroke length} = \frac{(v^2)}{2gN_g \eta} \quad [31], \quad v = 2.66 m/s$$

Where, a stroke length of 150 mm (Model: Thomson HD12B160-0400CNO1EEM), $N_g =$ Landing Gear Load Factor = 3, $\eta =$ Shock absorber efficiency = 80%, g is the gravitational constant (N/ kg) and v is the touch down velocity. Hence, the maximum touchdown velocity that the shock absorber can withstand is 2.66m/s. The maximum displacement of the landing gear can be calculated by the following equation:

$$(Eqn 3.2) x(t) = (C_1 + C_2 * t)e^{-W_n t} \quad [31]$$

The initial condition for the shock absorber is defined as $F = mg = kx = 105kN$, where k is the spring stiffness (700000 N/m). By substituting the initial condition into Eqn 3.2, the maximum time for maximum displacement of the shock absorber can be further calculated by using equation 3.3.

$$(Eqn 3.2) t = \frac{1}{W_n} x \left(1 + \frac{g}{W_n} x \left(\frac{1}{v - \frac{g}{W_n}} \right) \right), \quad \text{Max Time: } 0.1139 s$$

Where $W_n =$ Natural Frequency = $\sqrt{\frac{k}{m}} = 12.47$, $g =$ gravity = $9.81 m/s^2$.

e. BRAKING CALCULATIONS –The braking disc inside the wheel had a diameter of 5 inch and provides a dynamic torque of around 10000in-lb =1130Nm, and a breaking force of 1780N. A total of 5 breaking assembly, 1 on the front wheel and 2 on each of the back wheels (5 in total).

$$(Eqn 4.1) \quad K. E_{INITIAL} = Work Done_{FRICTION} + Work Done_{BRAKE}$$

Kinetic energy of the aircraft when it land: **5400000 J**, Drag Force provide by the wings: **2724 N**, Drag Force provide by the aircraft: **1029 N**, Total Break Force provide by the break: **8898 N**. If we assume the aircraft lands without decelerating, total distance required for the aircraft to stop is **427m**.

f. ACTUATOR RETRACTION & EXTENSION CALCULATIONS –The force required by the actuator when retracting and deploying the landing gear is required to select a suitable actuator.

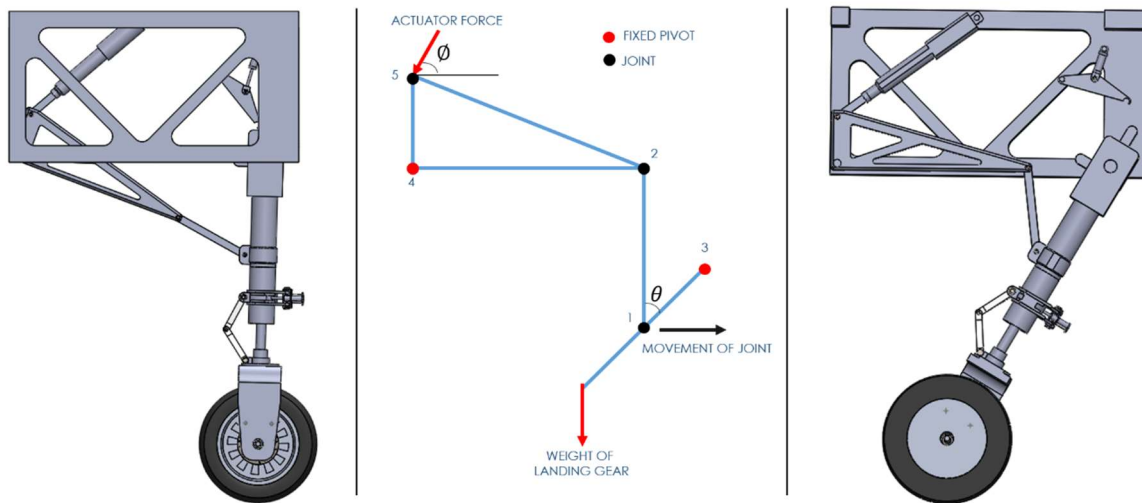


Figure 2.2.5- The diagram on the left, shows the landing gear structure, with actuator at full extension. The diagram in the middle shows the free body diagram analysis for the force required by the landing gear, take at one position. The model on the right shows the cross-sectional view of the free-body diagram position.

The dry weight of the landing gear strut assembly was calculated to be **26.4 kg** (including strut, shock absorber, braking system, wheel, tyre etc.). Firstly, the force required at the fixed pivot 3 was calculated using equation 1.1, then the force required at the actuator was calculated:

$$(Using Eqn 1.2 Moment about pivot 3) \quad F_1(\sin(\theta_1) \times x_1) = W(\sin(\theta_2) \times x_2) \quad F_1 = 666.8 N$$

$$(Using Eqn 1.2 Moment about pivot 4) \quad F_1(\sin(90 - \phi) \times x_1) = F_{ACTUATOR}(\sin(\phi) \times x_3)$$

$$F_{ACTUATOR} = 2503.2 N$$

Where, W = weight, F₁ = force on first structural beam, F_{ACTUATOR} = force required by actuator to retract landing gear.

3. STRUCTURAL DESIGN

(i) QUALITATIVE DESCRIPTION - The design process started off by team members brainstorming and clarifying objectives together. The objectives of having hybrid power, private use and number of passengers would be the main considerations in the later design. During the design impact sessions, the weight, cost, materials, structural dimensions and other technical details were set, which were the design criteria used in the fuselage design.

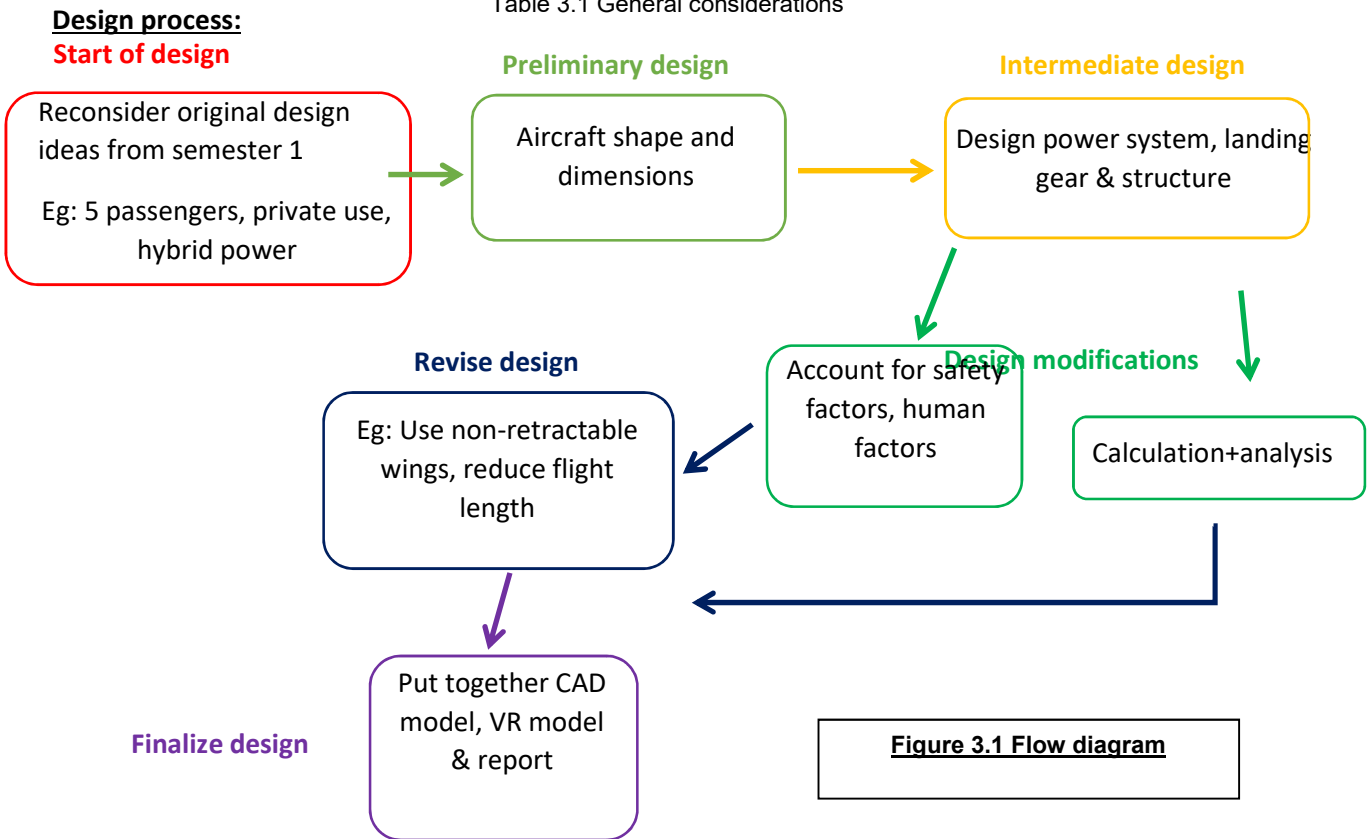
After setting sustainable goals from sustainability sessions (safe and affordable, energy efficient), these goals provided the team with a clear direction for our design. During the safety sessions, the potential dangers in the aircraft were realized. The fuselage is thus designed to be extra safe by accounting for load combinations including dead, live and wind loads during unfavorable scenarios while also withstanding large forces such as high wind pressures and landing impulsive force.

Then, necessary changes to the design are made (reduce flight length due to increase in weight/use non-retractable wings), as all disciplines come together and work on the final design. Finally, the design is finalized and all technical details and modelling are done.

(ii) QUANTITATIVE DESCRIPTION

Name	Description	Remarks
Dead Load (DL)	Battery – 5296 N (540 kg) Engine – 2746 N (280 kg) Fuel – 490 N (50 kg) Chair+monitor+desk – 686 N (14×5=70 kg) Fuselage self-weight – 15524 N (1583 kg) Front wing – 5543 N (610 kg) Back wing – 6276 N (910 kg) Front/back landing gear – 1961 N (200 kg)	Fuselage weight is spread across entire aircraft Sample calculations in appendix
Live Load (LL)	Passengers+luggage – 3923 N (80×5=400 kg) Max landing Impulse – 105 kN	-
Wind Load (Wind)	Max longitudinal wind load – 57 kN	-
LC1 (arch)	1.35DL + 1.5Wind	Load factors as stated in the Eurocode
LC2 (truss)	1.35DL + 1.5LL	
Carbon Fiber Reinforced Plastic	High strength-to-weight ratio High Fatigue strength	-
Aluminium Composite	Light Weight Ductile Cheap	-
Glass Composite	See through Increased strength	-

Table 3.1 General considerations



(iii) MODEL

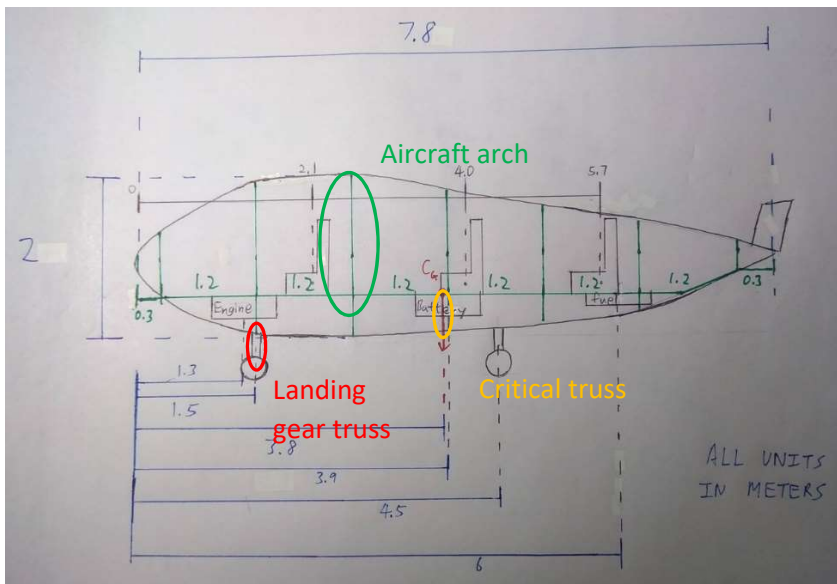


Figure 3.2-Overall model

Note that load combinations are not applied here yet, but would be in final calculation and analysis part.

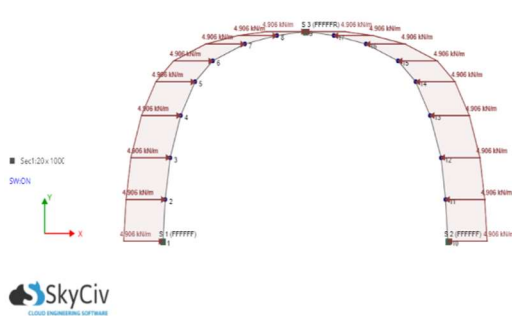


Figure 3.3 Aircraft arch (critical) – green circle in model

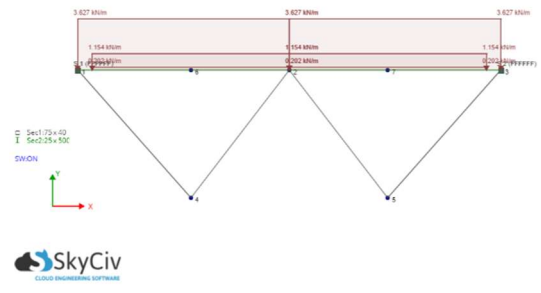


Figure 3.4 Normal truss (critical) – orange circle in model

Figure 3.3 shows a glass made arch (weakest material in aircraft) under critical loading. The longitudinal wind speed is maximum ($U_{max}=U_{mean}+3\sigma=107\text{m/s}$), which corresponds to a wind pressure per meter depth of 4.906 kN/m. (Calculations in appendix) This arch is also going to take the largest wind force as its cross-sectional area is the largest (1m tall & 1.6m wide). The figure 3.4 shows the truss underneath the deck under critical loading. This part of the truss (at 3.9m from front) is resisting the largest amount of load from deck (See appendix). At this point, the dimensions are assumed to be the greatest (0.44m tall & 1.46m wide) throughout the aircraft length.

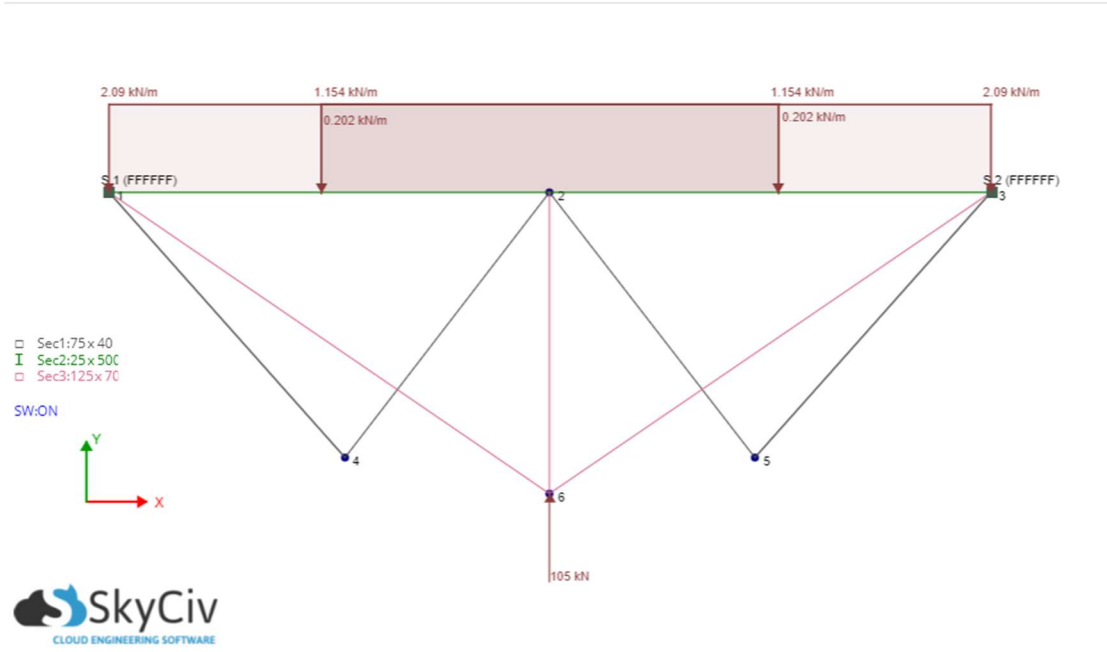


Figure 3.5 Front landing gear truss – red circle in model

The figure shows the truss of front landing gear under deck. In addition to dead/live loads on the deck, it is also designed to withstand the enormous amount of landing impulsive force – 105 kN bore by the front landing gear.

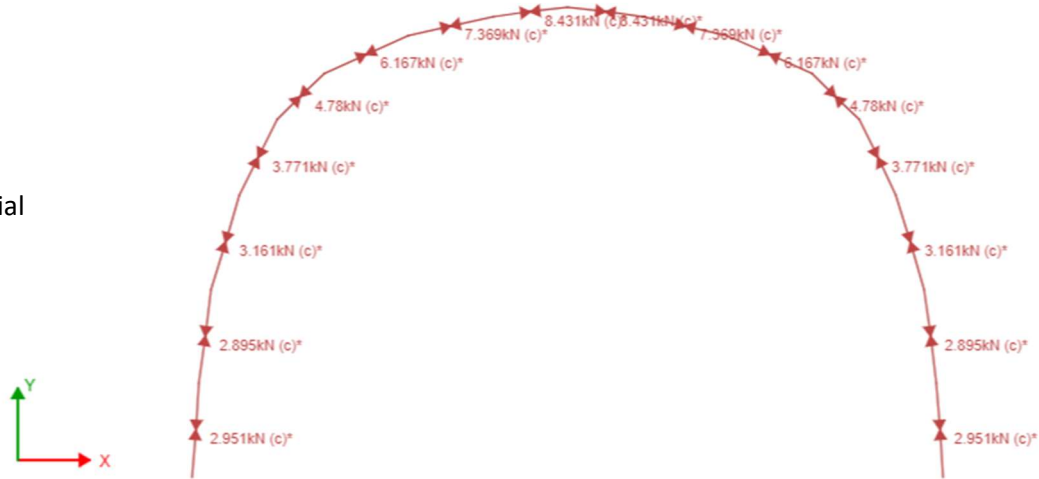
Each arch cross section has 2 fixed supports welded to the sides of the fuselage, restraining translation and rotation. A pinned support is placed at the top in the form of a longeron to allow slight deflections at the top of the arch and further increase structural strength. Each truss has 2 fixed supports welded to the sides.

(iv) ANALYSIS: DESIGN

Aircraft arch

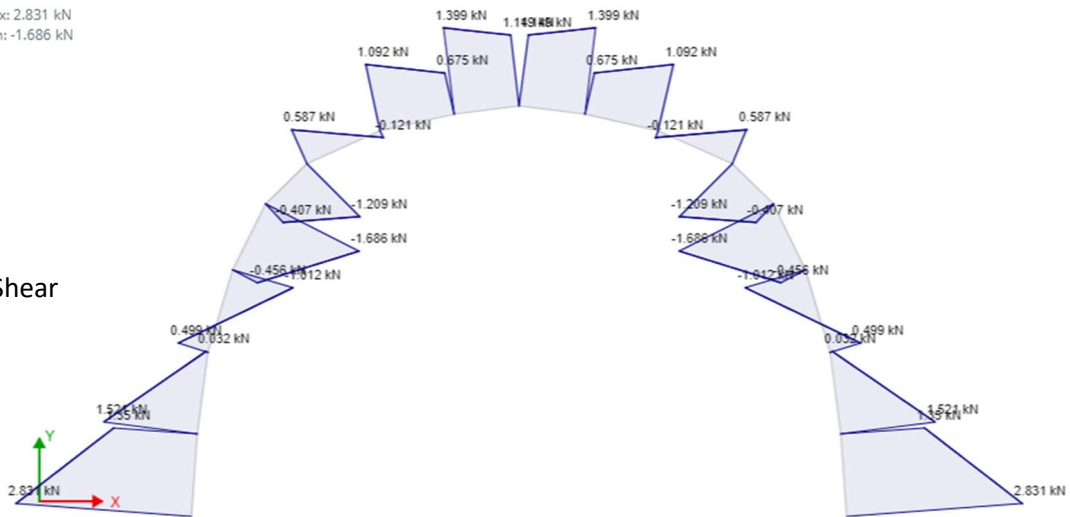
Max: 8.431 kN
Min: 2.836 kN

Axial



Max: 2.831 kN
Min: -1.686 kN

Shear



Max: 0.229 kN-m
Min: -0.402 kN-m

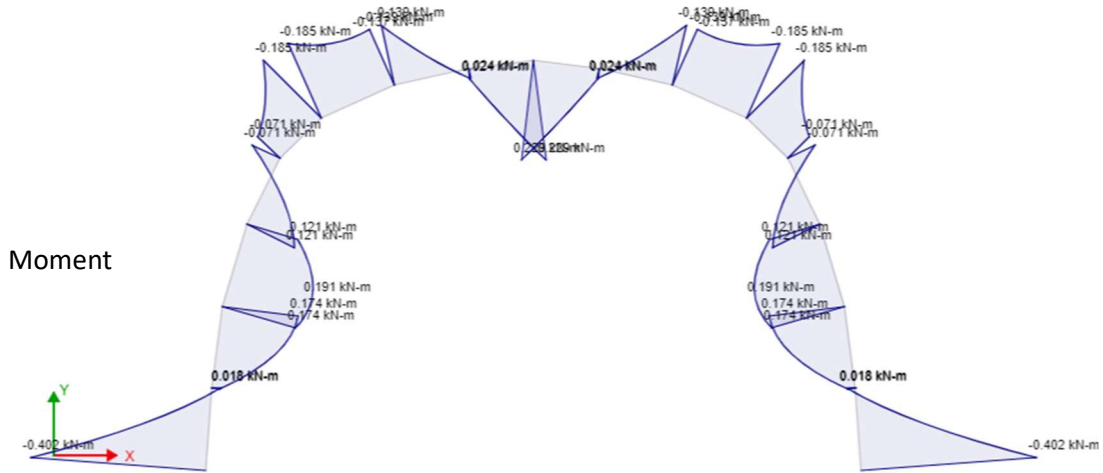
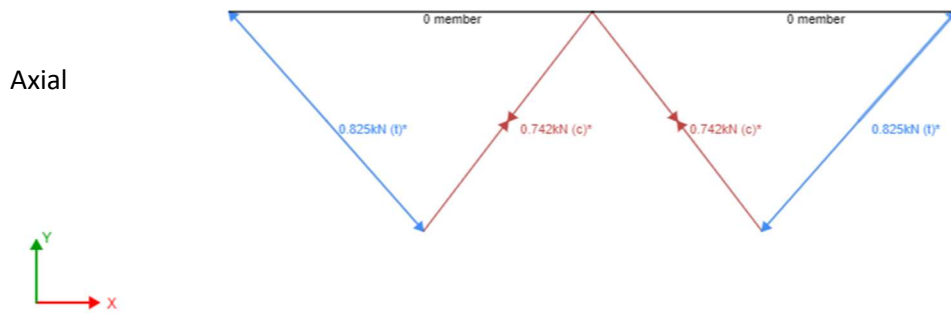


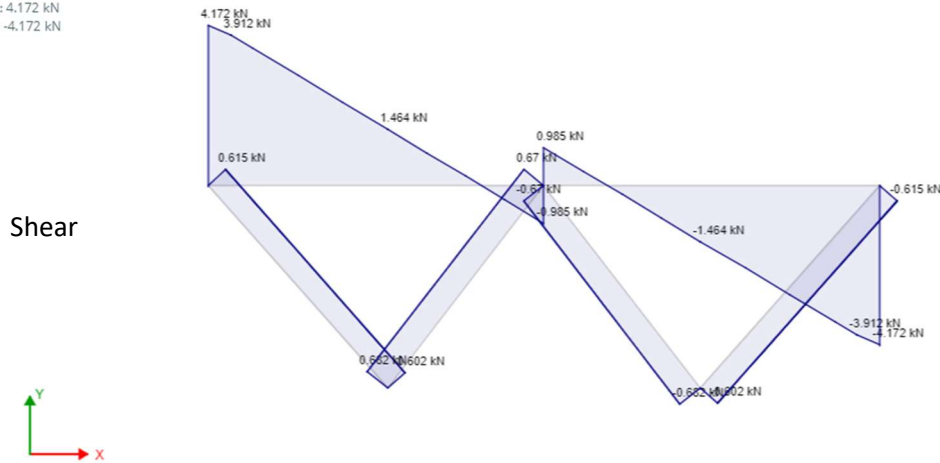
Figure 3.6-3.8 Diagrams of internal forces-aircraft arch

Normal truss (critical)

Max: 0.742 kN
Min: -0.825 kN



Max: 4.172 kN
Min: -4.172 kN



Max: 0.376 kN-m
 Min: -0.917 kN-m

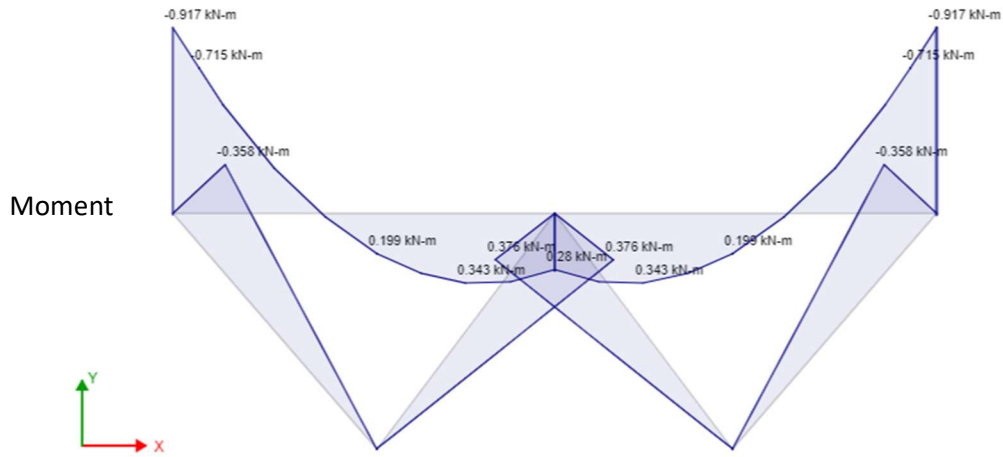
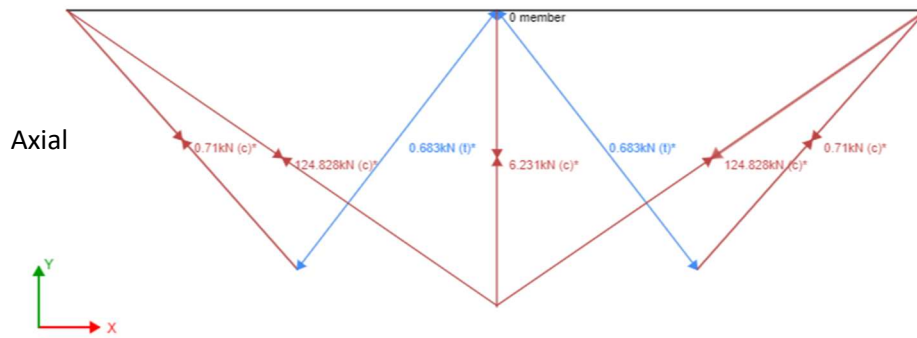


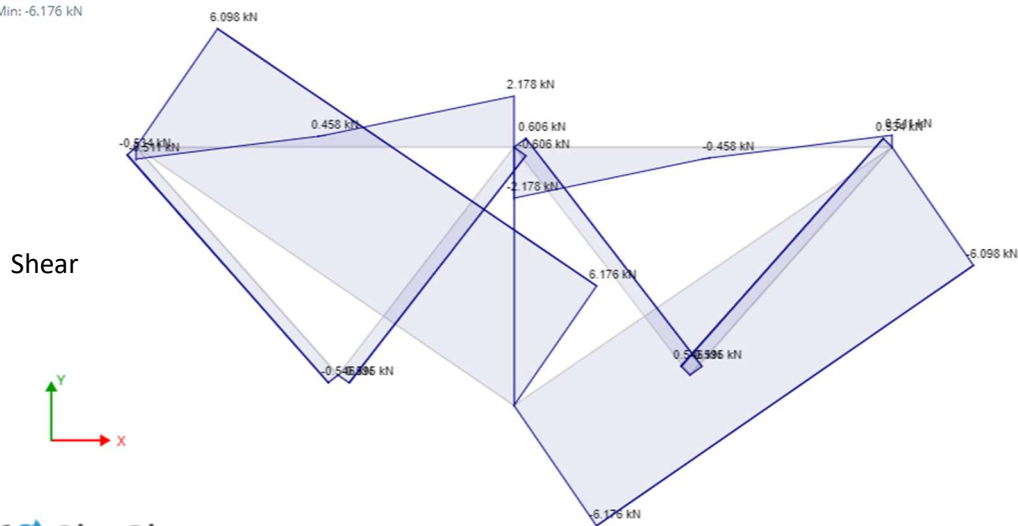
Figure 3.9-3.11 Diagrams of internal forces-normal truss (critical)

Landing gear truss

Max: 124.828 kN
 Min: -0.683 kN



Max: 6.176 kN
 Min: -6.176 kN



Max: 2.438 kN-m
Min: -2.449 kN-m

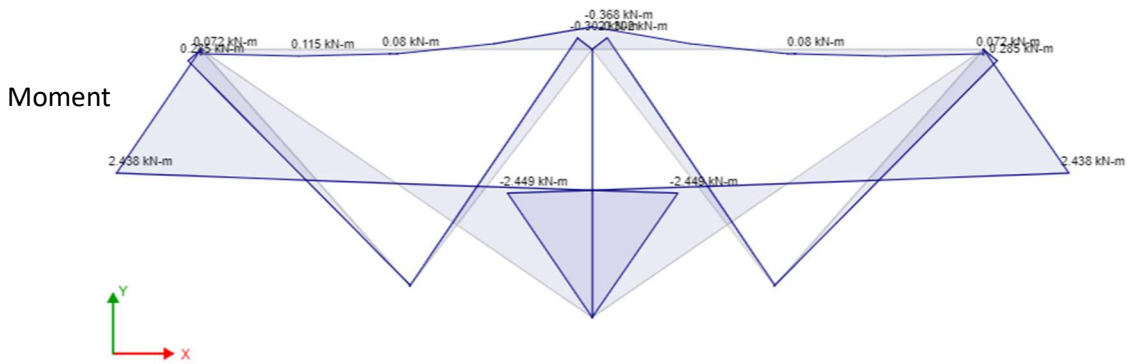
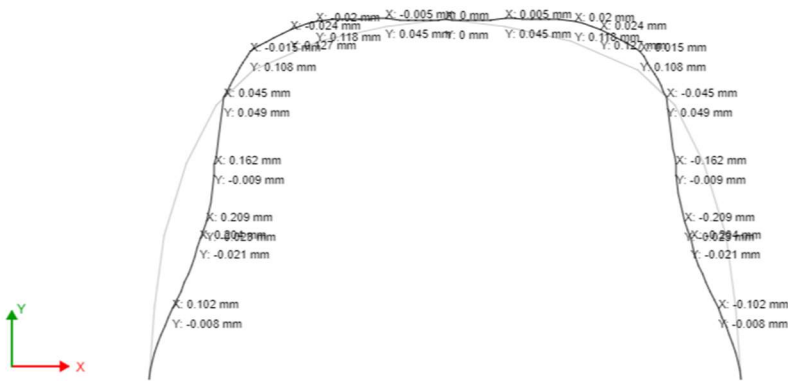


Figure 3.12-3.14 Diagrams of internal forces-landing gear truss

Deformation graphs

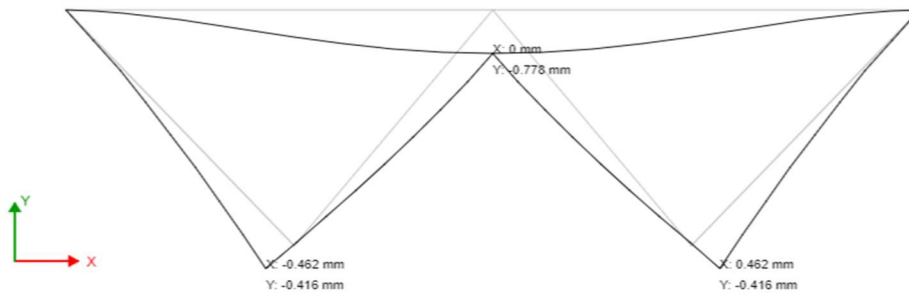
Max: 0.21 mm
Min: 0 mm

Aircraft arch

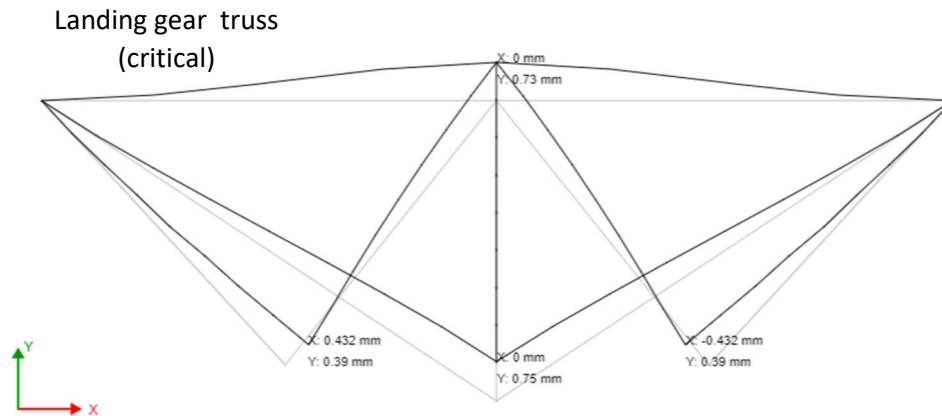


Max: 0.778 mm
Min: 0 mm

Normal truss (critical)



Max: 0.75 mm
Min: 0 mm



After accounting for load combinations, the aircraft arch resulted in a 1% deformation, which is within the elastic region of glass composites. The same goes for carbon fiber. There is a deformation of up to 3%, which is within the elastic range. This shows that the materials are still within elastic range even when using critical loads and load combinations. Therefore excessive deflection will not occur to the structure.

Having the dimensions, cost and weight in mind, the design process started off by estimating critical loads and scenarios the aircraft would face. Using software such as SkyCiv and applying load combinations from Eurocode, the software produces internal member forces, deflection etc. The obtained results are then used to re-evaluate and revise the existing model such as using stronger materials or changing shapes and dimensions of sections. The structural design is then finalized and merged with the model of all disciplines.

Final Sections (mm, mm², mm⁴)

Sections 1-3 refer to figure 3.4-3.5, section 4 refer to figure 3.3 arch

Section	Material	Shape	D×W	Shear area z	Shear area y	Torsion Radius
1(truss)	Aluminium	Hollow Rectangular	75×40	647.65	246.09	29.364
2(truss)	CFRP	I-Beam	25×500	6192.0	78.287	25.977
3(truss)	Aluminium	Hollow Rectangular	125×70	2136.4	869.17	51.232
4(arch)	Glass Composite	Rectangular	20×1000	16667	17455	20.784
Section	Centroid y	Centroid z	Area	I _y	I _z	J
1(truss)	37.5	20	989.00	232170	639239	593924
2(truss)	12.5	250	7265.0	108472000	553260	733546
3(truss)	62.5	35	3312.3	2281450	5895410	5700280
4(arch)	10	500	20000	1666670000	666667	2626390

Table 3.2- Table of final sections

CFRP=Carbon fibre reinforced plastic

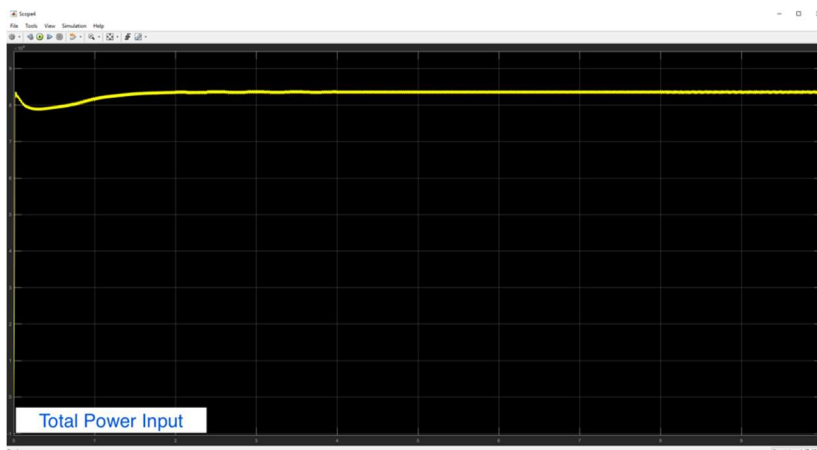
A load combination was set referring to the Eurocode to address ULS of the structure. As wind and live load does not ever appear in the same calculation (refer to appendix), the most unfavorable design scenario is $1.35DL+1.5LL$ or $1.35DL+1.5Wind$ with no exception as listed in the quantitative description. According to the graphs of member forces, the strengths of materials used are strong enough to withstand the different types of yielding and have acceptable deformation. For the SLS, the load factors are all equal to 1. Using the yield strength of materials, we can be sure that the structural loads are within the range of permissible values and the aircraft structure is serviceable under normal use.

4. APPENDIX

Inputs and Outputs

<provide an analysis of your electrical circuit behavior with reference to voltage, current, power, and other signals. This may include other domains you have chosen to model e.g. mechanical for the load.
– 100 words max>

Total power input is measured using a voltage measurement, a current measurement, and a power measurement. As shown in the graph below, the total power input from the fuel cells is approx. 820kW.



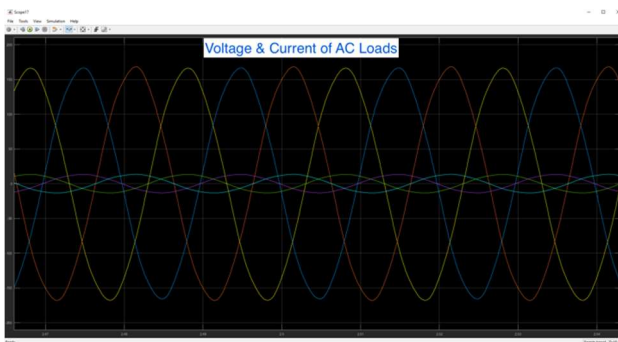
The total power consumed by the AC and DC loads varies against time. More power is consumed to start the DC motors, then their power requirement decreases dramatically (Gaser, and Kavanaugh, 1991). On the other hand, for AC loads, the sum of their power output increases against time.





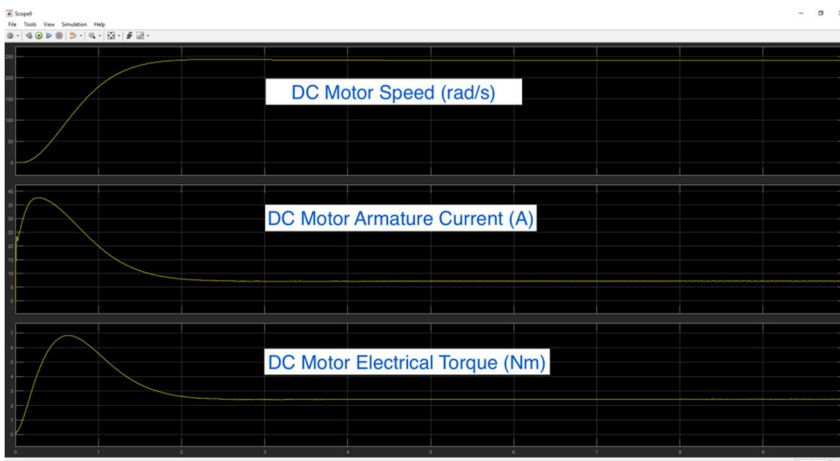
AC Loads Monitoring

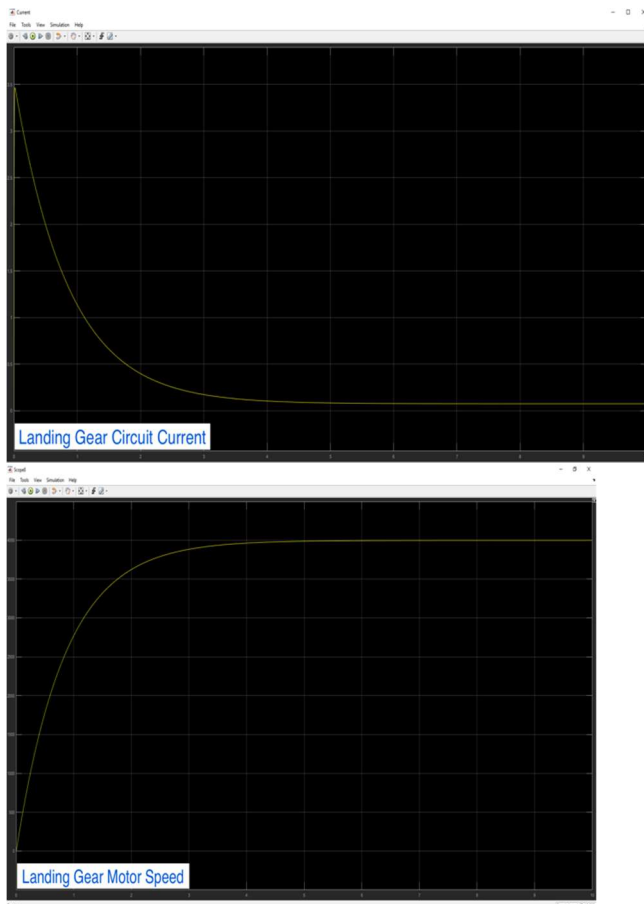
The graph below shows that the power generated by the hydrogen peroxide fuel cell is converted to a three-phase AC source.



DC Loads Monitoring

The behavior of the DC motor is shown below. Initially, the motor was not activated, therefore the at the beginning the electrical torque is higher. Then the motor starts accelerating until its limit. The armature current decreases as the speed increases. (Glowacz, et al, 2015)





Energy Efficiency

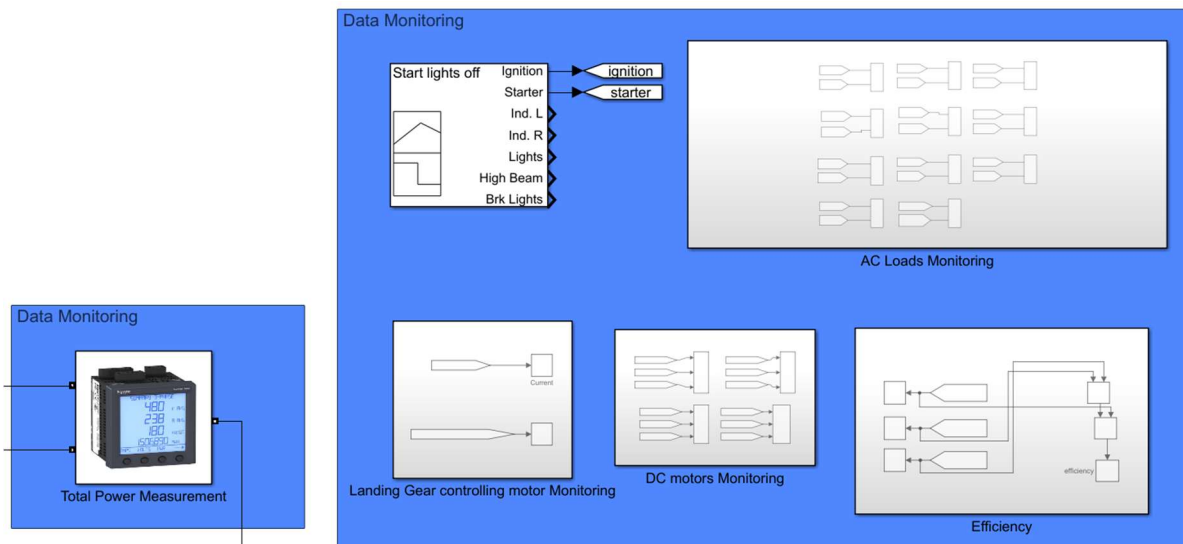
As shown below, the power efficiency remains approx. 60%. The power losses can be concluded as follows:

1. During the power conversion process, the waveform is filtered by capacitors, resistors and a transformer. In order to allow the basic parts of the waveform to successfully reach the output, normally a low pass filter is applied. These electronics might consume a considerable amount of power during the conversion. In this design, the three-phase inverters are implemented thus the losses are even higher. (Brown and Dell, 1999)
2. For DC motors, the non-ideal features include field, viscous friction and Coulomb friction torque (Famouri and Cathey, 1991).
3. For AC loads, extra resistors and inductors are used to simulate the losses caused by active and reactive power in the protection devices, cables, and wires.
4. The losses in the alternator include:
 - Friction losses: due to the rotor or the blowers.
 - Core losses: hysteresis and eddy currents
 - Stray load losses: due to magnetic flux distribution, harmonic and eddy currents. (Sharkh, 1999; Klang, 2002)

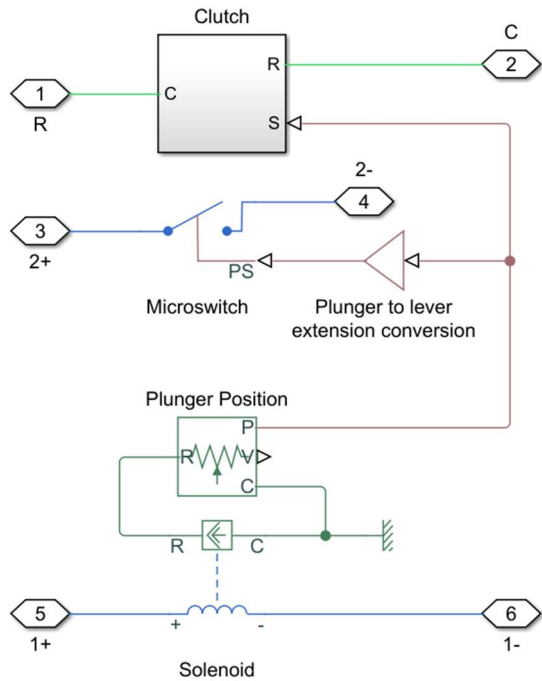


Appendix

Monitoring System



Starter Solenoid Details



MECHANICAL APPENDIX

If the thruster were pointing forward, minimum speed required to maintain the flying height:

$$\text{Lift force } F_L = \frac{1}{2} \rho C_L A V^2$$

$$\text{Weight } W = Mg$$

$$\text{Drag Force } F_d = \frac{1}{2} \rho C_d A V^2$$

- ρ = Density of air (1.225)
- C_L = Lift coefficient
- A = Area of total wing span
- V = Speed of the aircraft relative to the flow
- M = Mass of the aircraft
- g = Gravitational acceleration

For the aircraft to maintain a constant height, the Lift force must be equal to the weight of the aircraft.

Drag force acting on the main body can be estimated by first estimating the wing speed:

$$U_{average} = U_{10} \left(\frac{Z}{10} \right)^\alpha$$

- U Average wing speed at target height
- U_{10} Wind speed at 10m height= 30km/h
- Z Height of the aircraft= 310m
- α terrain index= 0.3

The average wind speed at 310m height will be 23.3m/s. Maximum flight speed is 250km/h, and our aircraft had a drag coefficient of 0.7.

$$\text{Maximum Drag Force acting on the body} = \frac{1}{2} \rho C_d A V^2 = 10620N$$

The total drag force acting on the wings can be derived using above formulas:

$$\text{Total Drag Force}_{\text{Wings}} = \frac{C_D}{C_L} Mg$$

We can get the lift and drag coefficient from the following diagram showing the values for aspect ratio of 6:1

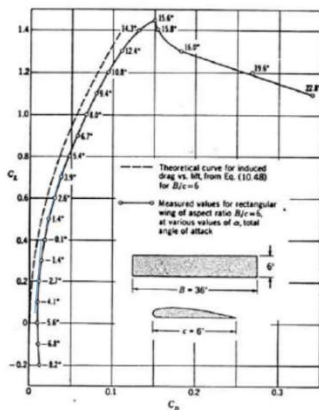


Table : Lift against Drag coefficient correspond to aspect ratio of 6

A table can be then filled to represent the total drag force acting on the wings.

Flight speed (km/h)	Flight Speed (m/s)	Lift coefficient	Drag Coefficient	Total Drag force on wings	Angle of attack	Drag Force acting on body	Total Drag Force
180	50.55	1.45	0.15	4566.7	15.6	6734.4	11301.08
200	55.55	1.2	0.095	3495	10.8	7679.1	11174.10
250	69.44	0.77	0.04	2303.96	1.4	10620	12923.96

Static load:

When the aircraft is static on the ground, the sum of moment acting on the aircraft is 0,

$$\text{Force of the front wheel} * 2.4 = 2 * \text{Force of the back wheels} * 0.6$$

$$\text{Sum of reaction force acting on the aircraft} = \text{Weight of the aircraft} = 45000(9.81)$$

The force acting on each of the landing gear were all equal to 14715N.

Static load:

When the aircraft is static on the ground, the sum of moment acting on the aircraft is 0,

$$\text{Force of the front wheel} * 2.4 = 2 * \text{Force of the back wheels} * 0.6$$

Sum of reaction force acting on the aircraft = Weight of the aircraft = 45000(9.81)

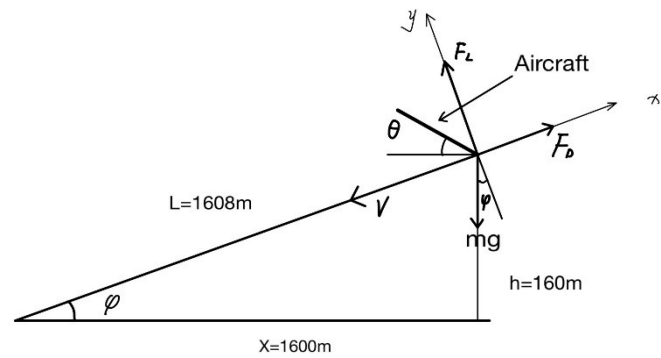
The force acting on each of the landing gear were all equal to 14715N.

$\theta = 10^\circ$, $\varphi = 5.71^\circ$, $h = 10m$ and glide ration equal to 10, which means $L = 1608m$. From the graph, it can be got that

$$\alpha = \theta + \varphi = 10 + 5.71 = 15.71^\circ$$

$$\begin{aligned} F_L &= \frac{1}{2} \rho_{air} C_L V^2 A \\ &= 0.5 \times 1.225 \times 1.45 \times 50.5^2 \times 19.5 \\ &= 44166N \end{aligned}$$

$$F_D = 4569N$$



Where $\rho_{air} = 1.225kg/m^3$, $V = 50.5m/s$ represents the speed that aircraft starting gliding, $A = 9m \times 1.5m + 6m \times 1m = 19.5m^2$ is the area of all the wings and α is the angle of attack.

From the graph, it shows that $C_D = 0.15$, $C_L = 1.45$, where C_D is the coefficient of drag and C_L is the coefficient of lift.

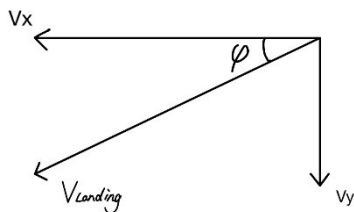
Thus $F_L = mg \cdot \cos(\varphi)$ which represents a balance in Y axis.

$$a_1 = \frac{mg \cdot \sin(\varphi) - F_D}{m} = \frac{4500 \times 9.81 \times 0.0995 - 4569}{4500} = -0.04m/s^2$$

Where a represents the acceleration in X axis.

$$V_{landing}^2 - V^2 = 2a_1L$$

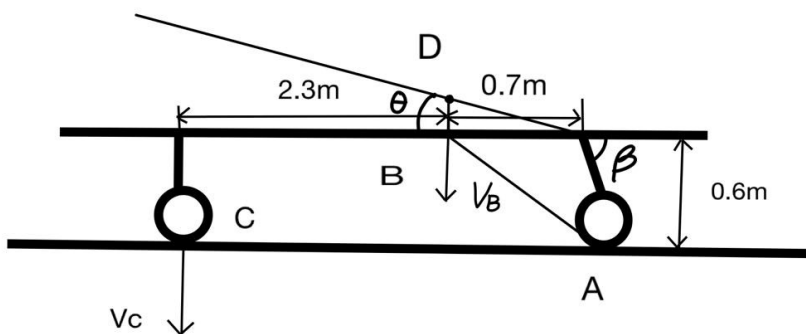
So it can be got that $V_{landing} = 49.2m/s$, where $V_{landing}$ is the speed of landing.



$$V_x = V_{landing} \cdot \cos(5.71) = 49.2 \times 0.995 = 49m/s$$

$$V_y = V_{landing} \cdot \sin(5.71) = 4.9m/s$$

Where V_x represents the speed of sliding on the ground and V_y is the vertical speed of landing.



$C_{L2} = 1.2$, $C_{D2} = 0.095$
when the angle of attack is 10° , So when the aircraft is sliding on the ground.

$$F_{L2} = \frac{1}{2} \rho_{air} C_{L2} V^2 A = 0.5 \times 1.225 \times 1.2 \times 49^2 \times 19.5 = 34412N$$

$$F_{D2} = \frac{C_{D2}}{C_{L2}} \cdot F_{L2} = \frac{0.095}{1.2} \times 34412 = 2724N$$

$$a_2 = \frac{mg - F_{L2}}{m} = \frac{4500 \times 9.81 - 34412}{4500} = 2.163m/s^2$$

Where F_{L2}, F_{D2}, a_2 represents lift force, drag force and the acceleration of central gravity when aircraft is sliding on the ground.

$$V_B^2 = 2a_2 L_{BD}$$

$$V_B = \sqrt{2 \times 2.163 \times 0.1215} = 0.725m/s$$

Where $L_{BD} = 0.7m \times \sin(10^\circ) = 0.1215m$ is the distance that central gravity moves before front wheel get touch with ground, V_B is the velocity of central gravity when front wheel get touch with ground.

Thus, $\beta = 84^\circ$ which is the angle between chassis and back wheel, $L_{AB} = 0.97m$ and $L_{AC} = 3m$, so

$$V_C = \frac{L_{AC}}{L_{AB}} \cdot V_B = \frac{3}{0.97} \times 0.725 = 2.24m/s$$

Where V_C is the vertical speed of front wheel when it touch with ground.

CIVIL APPENDIX

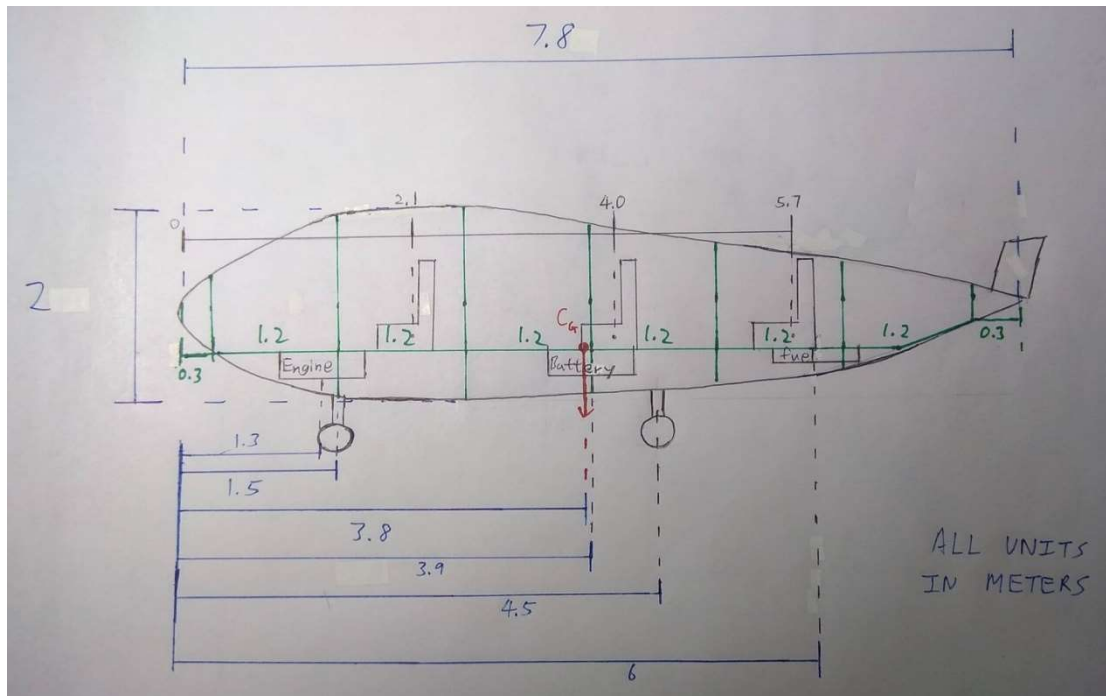


Figure 3.2 Overall model

$$\begin{aligned}
 \text{Fuselage self weight} &= \left[\underbrace{(147.4 \cdot 7.8 \cdot 0.7)}_{\substack{\text{Mass per meter} \\ \text{top arch (glass) composite}}} + \underbrace{(74 \cdot 7.8 \cdot 0.8)}_{\substack{\text{volume factor} \\ \text{bottom arch} \\ \text{(aluminium composite)}}} + \underbrace{43.2 \cdot 6}_{\substack{\text{normal truss} \\ \text{(aluminium)}}} + \underbrace{57.2}_{\substack{\text{Landing gear truss} \\ \text{(aluminium + carbon fiber)}}} \right] \times 9.807 \\
 &= 1583 \cdot 9.807 \\
 &= 15524 \text{ N}
 \end{aligned}$$

Figure 3.18 Fuselage self-weight calculation

Wind pressure

flying height = 310 m

$$\bar{V}(z) = \bar{V}_{10} \left(\frac{z}{10} \right)^\alpha$$

Assuming very high wind speed at 10m above ground $\bar{V}_{10} = 70 \text{ km/h} = 19.44 \text{ m/s}$

Using type IV terrain (worst case)
 $\alpha = 0.3$
 $I_n = 0.32$
 $H_0 = 510$

$$\bar{V}(310) = \bar{V}_{10} \left(\frac{310}{10} \right)^\alpha = 19.44 (31)^{0.3} = 54.46 \text{ m/s} \leftarrow \text{mean wind speed}$$

Accounting for maximum wind speed $I_n = \frac{G_u}{\bar{V}(z)}$

Longitudinal G is max.

$$G_u = I_n \cdot \bar{V}(310) = 0.32 \cdot 54.46 = 17.43 \text{ Nm}^{-2}$$

Wind Load = pressure / side Area

$$\text{Wind Load} = 4906 \cdot (2 \cdot 7.8 \cdot 0.75) = 57.4 \text{ kN}$$

∴ peak $V = \bar{V}(310) + 3G_u = 54.46 + 3 \cdot 17.43 = 106.75 \text{ m/s}$

peak pressure = $\frac{1}{2} C_D \rho V^2$

$C_D = 0.7$

$$= \frac{1}{2} \cdot 0.7 \cdot (1.23) (106.75)^2 = 4906 \text{ Nm}^{-2}$$

∴ Wind pressure per meter depth = $4906 \text{ Nm}^{-2} \cdot 1 \text{ m} = 4906 \text{ Nm}^{-1}$

Figure 3.19 Wind pressure calculation

Normal truss (critical) - 3.9m from front.

Dead Load (DL) $\times 1.35$

Battery - 540kg

2 (Chair + motor + desk) - 14kg $\times 2$

Live Load (LL) $\times 1.5$

passenger + luggage - 80kg $\times 2$

Used in analysis

Actual Load

Allocated Load

Deck 1.6m

1.5m

0.5m

0.47m

0.68m

0.39m 0.34m 0.34m 0.39m

1.46m

Note: software will apply load combinations during analysis automatically.

Force per meter depth ← Input in software

Battery - $\frac{5296}{1.46} = 3627 \text{ kN/m}$

Chair + motor + desk - $\frac{274.6}{0.68 \cdot 2} = 202.02 \text{ kN/m}$

passenger + luggage - $\frac{1569}{0.68 \cdot 2} = 1154 \text{ kN/m}$

Figure 3.20 Normal truss load combinations and software input data

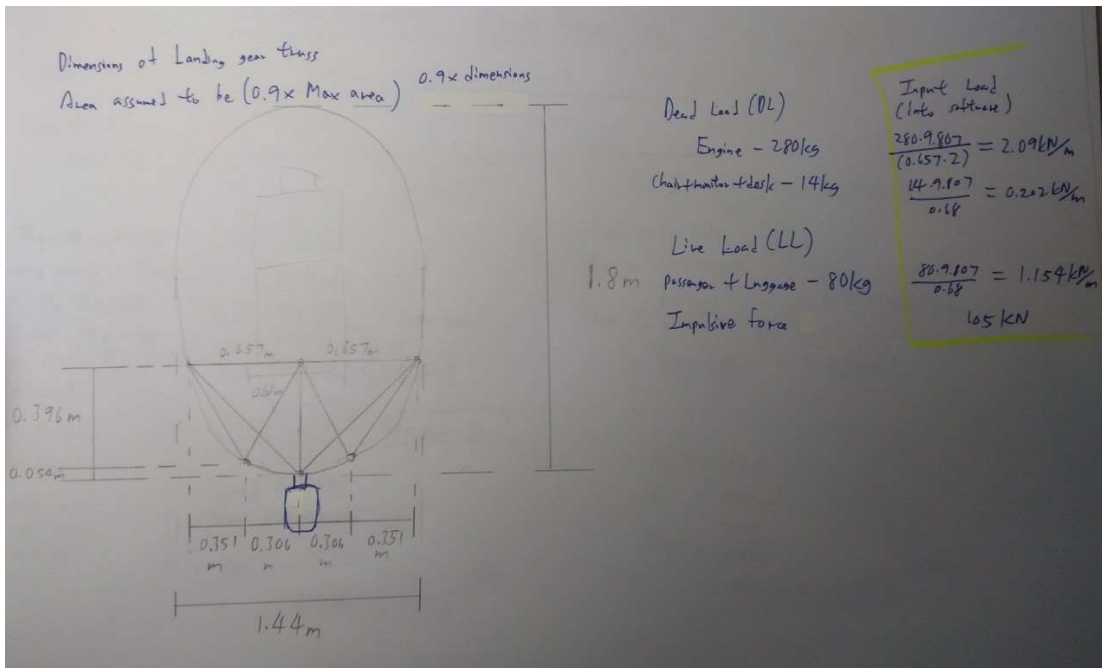


Figure 3.21 Landing Gear truss calculation

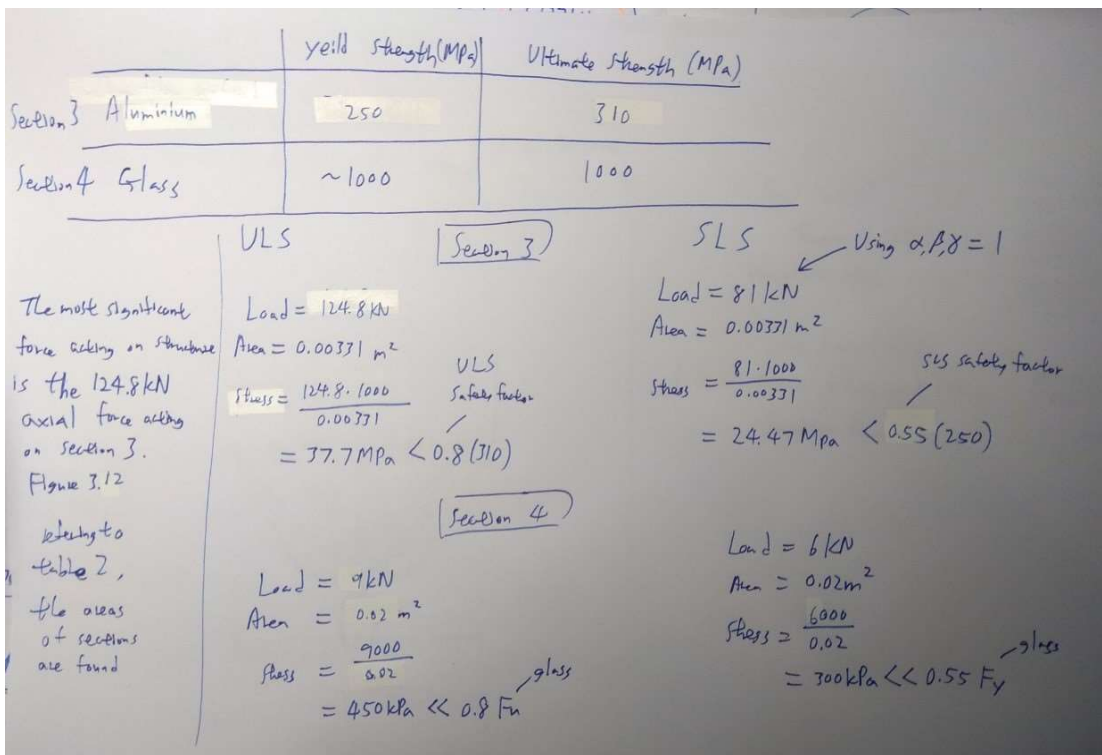


Figure 3.22 ULS/SLS considerations

Max: 80.951 kN
Min: -0.44 kN

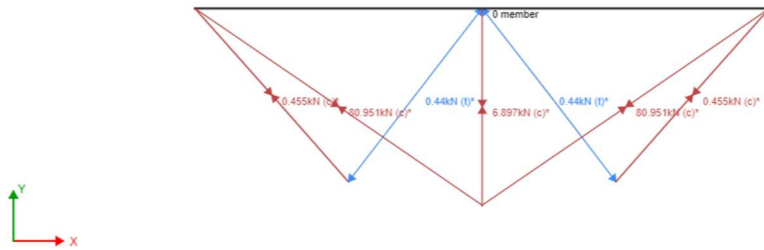


Figure 3.23 SLS axial loads – landing gear truss(without load combinations)

Max: 5.628 kN
Min: 1.939 kN

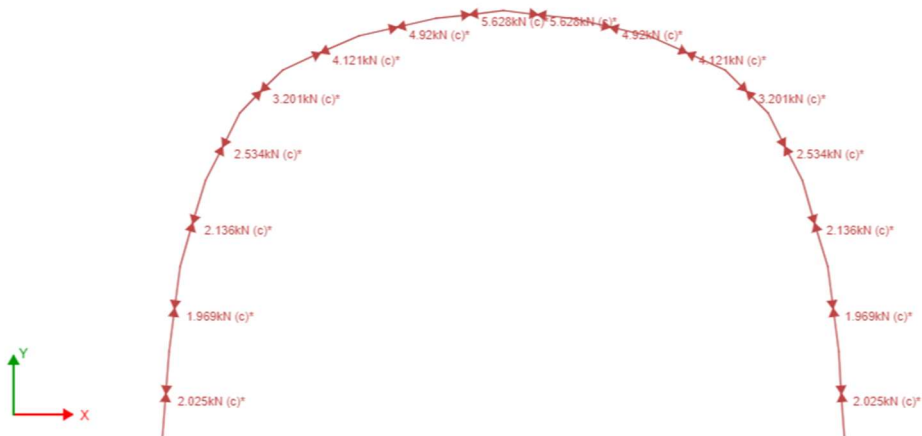


Figure 3.24 SLS axial loads – arch (without load combinations)

5. REFERENCE

- [1] Kurohane, K., Senjyu, T., Uehara, A., Yona, A., Funabashi, T. and Kim, C.H., 2010, June. A hybrid smart AC/DC power system. In *2010 5th IEEE Conference on Industrial Electronics and Applications* (pp. 764-769). Ieee.
- [2] Berényi, A., Belluscio, M., Mao, D. and Buzsáki, G., 2012. Closed-loop control of epilepsy by transcranial electrical stimulation. *Science*, *337*(6095), pp.735-737.
- [3] Tartakovsky, B. and Guiot, S.R., 2006. A comparison of air and hydrogen peroxide oxygenated microbial fuel cell reactors. *Biotechnology progress*, *22*(1), pp.241-246.
- [4] Holtz, J., 1994. Pulsewidth modulation for electronic power conversion. *Proceedings of the IEEE*, *82*(8), pp.1194-1214.
- [5] Boniol, F. and Wiels, V., 2014, June. The landing gear system case study. In *International Conference on Abstract State Machines, Alloy, B, TLA, VDM, and Z* (pp. 1-18). Springer, Cham.
- [6] Bessette, R.R., Cichon, J.M., Dischert, D.W. and Dow, E.G., 1999. A study of cathode catalysis for the aluminium/hydrogen peroxide semi-fuel cell. *Journal of Power Sources*, *80*(1-2), pp.248-253.
- [7] Yamanaka, I., Onizawa, T., Takenaka, S. and Otsuka, K., 2003. Direct and continuous production of hydrogen peroxide with 93% selectivity using a fuel-cell system. *Angewandte Chemie*, *115*(31), pp.3781-3783.
- [8] Dunn, B., Kamath, H. and Tarascon, J.M., 2011. Electrical energy storage for the grid: a battery of choices. *Science*, *334*(6058), pp.928-935.
- [9] McAlister, R.E., McAlister Tech LLC, 2009. *Multifuel storage, metering and ignition system*. U.S. Patent 7,628,137.
- [10] Welches, R.S., Semikron Inc, 2002. *Transformerless 3 phase power inverter*. U.S. Patent 6,404,655.
- [11] Dugan, R.C. and Santoso, S., 2003, September. An example of 3-phase transformer modeling for distribution system analysis. In *2003 IEEE PES Transmission and Distribution Conference and Exposition (IEEE Cat. No. 03CH37495)* (Vol. 3, pp. 1028-1032). IEEE.
- [12] Wibben, J. and Harjani, R., 2008. A high-efficiency DC–DC converter using 2 nH integrated inductors. *IEEE Journal of Solid-State Circuits*, *43*(4), pp.844-854.
- [13] Khoucha, F., Lagoun, S.M., Marouani, K., Kheloui, A. and Benbouzid, M.E.H., 2008, September. Hybrid cascaded H-bridge multilevel inverter motor drive DTC control for Electric Vehicles. In *2008 18th International Conference on Electrical Machines* (pp. 1-6). IEEE.
- [14] Bieber, P., Boniol, F., Boyer, M., Noulard, E. and Pagetti, C., 2012. New Challenges for Future Avionic Architectures. *AerospaceLab*, (4), pp.p-1.
- [15] Löfwenmark, A. and Nadjm-Tehrani, S., 2014, November. Challenges in future avionic systems on multi-core platforms. In *2014 IEEE International Symposium on Software Reliability Engineering Workshops* (pp. 115-119). IEEE.
- [16] Volk, K.R., Maxim Integrated Products Inc, 2000. *Step-up/step-down switching regulators and pulse width modulation control therefor*. U.S. Patent 6,087,816.

- [17] Squibb, G.F., Hewlett-Packard Development Co LP, 2007. *Pulse width modulation fan control*. U.S. Patent 7,211,977.
- [18] Adams, J.A., 1971. A closed-loop theory of motor learning. *Journal of motor behavior*, 3(2), pp.111-150.
- [19] Bolognani, S., Bolognani, S., Peretti, L. and Zigliotto, M., 2009. Design and implementation of model predictive control for electrical motor drives. *IEEE Transactions on industrial electronics*, 56(6), pp.1925-1936.
- [20] Gaser, M. and Kavanaugh, R., Iskra Electromorji, 1991. *High speed, high power, single phase brushless DC motor*. U.S. Patent 5,041,749.
- [21] Glowacz, A., Glowacz, W. and Glowacz, Z., 2015. Recognition of armature current of DC generator depending on rotor speed using FFT, MSAF-1 and LDA. *Eksploracja i Niezawodność*, 17.
- [22] Brown, A.E., Dell Usa LP, 1999. *System and method for reducing power losses by gating an active power factor conversion process*. U.S. Patent 5,960,207.
- [23] Famouri, P. and Cathey, J.J., 1991. Loss minimization control of an induction motor drive. *IEEE Transactions on Industry Applications*, 27(1), pp.32-37.
- [24] Sharkh, S.A., Irenji, N.T. and Harris, M., 1999. Effect of power factor on rotor loss in high-speed PM alternators.
- [25]Klang, J.K., Midtronics Inc, 2002. *Alternator tester*. U.S. Patent 6,466,025.
- [26] Rosero, J.A., Ortega, J.A., Aldabas, E. and Romeral, L.A.R.L., 2007. Moving towards a more electric aircraft. *IEEE Aerospace and Electronic Systems Magazine*, 22(3), pp.3-9.
- [27] Marek, J. 2012. Actuators. Hydraulic vs Electromechanical Actuators. [Online]. 1(1), 2. [02 March 2019]. Available from: <https://www.manufacturing.net/article/2012/05/hydraulic-vs-electromechanical-actuators>
- [28] Thomsons, M.A.R.E.K. 2018. Thomson Linear Motion Optimised. Linear Actuators. [Online]. 1(1), 2. [02 March 2019]. Available from: <https://www.thomsonlinear.com/en/products/linear-actuators-products>
- [29] Ace, C.O.N.T.R.O.L.S. 2018. Shock Absorber. ACE Deceleration & Vibration Technology. [Online]. 1(1), 2. [15 February 2019]. Available from: <https://www.acecontrols.com/us/>
- [30] Jashay, P. 2019. Comline Auto Parts. Brake Discs - ADC1215V. [Online]. 1(1), 12. [12 February 2019]. Available from: <http://www.comline.uk.com/catalogue/ADC1215V>
- [31] Bosniceanu daniel, B.D. 2011. SOME ASPECTS REGARDING IMPACT ABSORBERS APPLIED ON AIRCRAFT LANDING GEARS. INTERNATIONAL CONFERENCE of SCIENTIFIC PAPER AFASES 2011. [Online]. 1(12), 1-7. [12 March 2019]. Available from: <http://www.afahc.ro/ro/afases/2011/eng/4.3/Bosniceanu.pdf>
- [32] Tolomatic, M.A.N.U.F.A.C.T.U.R.I.N.G. 2018. EXCELLENCE IN MOTION. Electric Linear Actuators. [Online]. 5(16), 12-70. [12 March 2019]. Available from: <https://www.tolomatic.com/>